2010

The Role of Synaptically Evoked Plateau Potentials in Retinogeniculate Development

Emily Dilger
Virginia Commonwealth University

The Role of Synaptically Evoked Plateau Potentials in Retinogeniculate Development

A dissertation submitted in partial fulfillment of the requirements for the degree of Doctor of Philosophy at Virginia Commonwealth University.

by

Emily K. Dilger, BS
Mary Washington College, 2004

William Guido, PhD
Professor
Department of Anatomy and Neurobiology

Virginia Commonwealth University
Richmond, Virginia
November, 2010

Acknowledgments

First and foremost, my gratitude goes out to my advisor, Dr. Bill Guido, for his unending support, patience and guidance. I was so lucky to have him take me into his lab and put up with me. He has really managed to get the right balance of guidance and independence, and has helped me mature into a young scientist. I would like to thank my committee who were always available: Dr. Jason Chen, for PCR equipment and techniques; Dr. Mike Fox, for advising on western blot problems; Dr. Rory McQuiston, for endless electrophysiology suggestions; and Dr. Carmen Sato-Bigbee, for hours of advice on everything from predoctoral fellowships to finding an advisor. I was also lucky to have amazing lab mates: I need to thank Dr. Thomas Krahe, an infinite source of troubleshooting and troublemaking; Tania Seabrook, who has become one of my best friends; Rana El-Danaf, especially for her reminders that were necessary for getting to class and her wonderful Lebanese food; and Dr. Chris Jurgens, a great resource for all types of knowledge. In addition, many others made this work possible: Dr. Hee-Sup Shin (Korean Institute for Science and Technology) for the β_3 null mouse, Dr. Kevin Campbell (University of Iowa) for the β_1, β_2 and β_4 antibodies, Dr. Duncan Morhardt (VCU) for the β_3 null retinal wave recordings and Frank Chen (VCU) for his PCR wisdom. I would also like to thank Dr. John

Povlishock and the entire Anatomy and Neurobiology Department at Virginia Commonwealth University, as well as Dr. John Bigbee, the Neuroscience Program Director.

I would like to thank my family for their constant love and support: my Dad, Dr. Jim Dilger, who is my role model; my Mom, Kate Dilger, who has been my confidence when I have none; my brother, Andrew Dilger and the rest of my extended family. I need to thank my friends Laura Desmond and Bess Krahn, who have always been only a phone call away. Finally, I need to thank my boyfriend and partner Shep Shapard, who should be receiving a PhD in 'How to be in a Relationship with Someone Receiving a PhD' for all the guff he has had to put up with over these years.

TABLE OF CONTENTS

LIST OF FIGURES AND TABLES

ABBRIVIATIONS

ACSF, artificial cerebral spinal fluid; AHP, afterhyperpolarization; AMPAR, α-amino-3-hydroxy-5-methyl-4-isoxazolepropionic acid receptor; BTDP, burst-time dependent plasticity; CaM, calmodulin; CaMK, CaM kinase; CaN, calcineurin; CNS, central nervous system; CRE, cAMP response element; CREB, CRE binding protein; CTB, cholera toxin subunit B; DAB, diaminobenzidine; dLGN, dorsal lateral geniculate nucleus; EPSC, excitatory post-synaptic current; EPSP, excitatory post-synaptic potential; IGL, intergeniculate leaflet; IP_3, inositol (1,4,5)-trisphosphate receptor; IPSP, inhibitory post-synaptic potential; MHC1, major histocompatability complex class 1; OT, optic tract; NMDAR, N-methyl-D-aspartic acid receptor; P, postnatal day; RGC, retinal ganglion cells retinal ganglion cell; SER, smooth endoplasmic reticulum;VGCC, voltage-gated Ca^{2+} channel; WT, wild type.

Abstract

THE ROLE OF SYNAPTICALLY EVOKED PLATEAU POTENTIALS IN RETINOGENICULATE DEVELOPMENT

By Emily K. Dilger, Ph.D.

A dissertation submitted in partial fulfillment of the requirements for the degree of Doctor of Philosophy at Virginia Commonwealth University.

Virginia Commonwealth University, 2010.

William Guido, PhD, Professor, Department of Anatomy and Neurobiology

We study the activity-dependent refinement of sensory systems by using the mouse retinogeniculate system as a model. Spontaneous retinal waves lead to robust excitatory post-synaptic activity in developing relay cells in the dorsal lateral geniculate nucleus (dLGN) of the thalamus and are reportedly needed to help guide the segregation of retinal inputs into eye-specific domains as well as for the pruning of extraneous retinal inputs onto single dLGN relay cells. The composition of retinally evoked post-synaptic activity activated by these retinal waves in dLGN is largely unknown, but based on our *in vitro* recordings, such activity seems well suited to activate large, long-lasting, high-amplitude depolarizations mediated by L-type Ca^{2+} channel activation, plateau potentials. Plateau activity prevails early in life, at the peak of retinogeniculate refinement, however, little is known about the factors that contribute to the activation of these events, or the potential role of plateau potentials in mediating activity-dependent remodeling. In this thesis, we examined the factors and stimulus conditions that lead to the activation of plateau activity. We found that many aspects of developing retinogeniculate

circuitry (e.g., the high degree of retinal convergence, the temporal summation of excitatory post-synaptic potentials, and the lack of inhibitory connections) seem to favor their activation at early postnatal ages. We then tested whether such activity is necessary for the refinement of retinal projections, as well as their functional connections onto dLGN cells. To address this, we took a loss-of-function approach and made use of a transgenic mouse that lacks the β_3 subunit of the L-type Ca^{2+} channel. These mutants have far fewer membrane-bound L-type Ca^{2+} channels and greatly attenuated L-type activity. In β_3 nulls, L-type plateau potentials are rarely observed in the dLGN, even at young ages or when repetitive pulses of electrical stimulation are applied to the optic tract. Although these mice have normal stage II and III spontaneous retinal waves, the retinogeniculate projections of β_3 null mice fail to segregate properly. In addition, the degree of retinal pruning is impaired. These results suggest that post-synaptic L-type Ca^{2+} channel activity is necessary to implement the activity-dependent refinement of the retinogeniculate pathway.

Introduction

The calcium ion regulates many aspects of cellular processing, from as early as fertilization, where Ca^{2+} waves initiate development, to controlling pattern formation and cellular differentiation, to proliferation and apoptosis in the adult (Berridge *et al*., 2000). Its role is particularly important in the development of the central nervous system (CNS), where it controls early synaptogenesis, guiding outgrowth in dendritic filipodia as well as forming and maintaining contacts with axons (Lu *et al*., 2009). These processes happen independent of synaptic transmission, guided instead by intrinsic genetic programming where Ca^{2+} insures correct diversity and numbers as well as the general placement of neurons and glia in the brain. Later in life, when experiences guide the refinement of neural connections, Ca^{2+} is the signal of choice for triggering the strengthening and maintenance of appropriate synaptic connections, and the elimination of inappropriate ones (Torborg & Feller, 2005). The importance of Ca^{2+} continues in adult plasticity where synapse-specific alterations mediate short-term and long-term changes in synaptic strength (Malenka & Bear, 2004). These effects can be local, including the

insertion or removal of glutamatergic receptors from the membrane, the functional alteration of synaptic proteins via posttranslational modifications such as phosphorylation, and the amount of those proteins via translation or degradation (Greer & Greenberg, 2008). In addition, Ca^{2+} influx can initiate signaling cascades that culminate in the nucleus and result in the activation of gene transcription and mediate various long-term changes in synaptic growth, maintenance and strength (Greer & Greenberg, 2008).

The cell is able to tightly regulate Ca^{2+} by maintaining low concentrations, thus limiting baseline Ca^{2+} noise and permitting rapid influxes that signal based on their amplitude, frequency and duration (Blackstone & Sheng, 2002). Ca^{2+} is also restricted spatially and temporally within the cell by high-capacity Ca^{2+}-binding proteins, efflux through Ca^{2+} pumps on the plasma membrane and compartmentalization in intracellular organelles such as the smooth endoplasmic reticulum (SER; Bardo *et al*., 2006). The SER holds Ca^{2+} at up to four times the cytosolic concentration (Bardo *et al*., 2006), and can release it throughout the cell including from dendritic spines, where the majority of excitatory synapses are located, in specialized compartments called the spine apparatus (Blackstone & Sheng, 2002). SER Ca^{2+} release comes from two types of receptors, ryanodine receptors, which are Ca^{2+} activated, and inositol (1,4,5)-trisphosphate receptors (IP_3), a metabolic by-product of phospholipase C activity linked to the stimulation of metabotripic glutamate receptors (Bardo *et al*., 2006).

The major source of Ca^{2+} influx, however, comes from the extracellular space. The glutamatergic NMDA receptors (NMDAR) are the typical candidate of choice for activity-dependent Ca^{2+} influx because, as well as being the predominant source of Ca^{2+} influx into spines (Blackstone & Sheng, 2002), they act as co-incident detectors, only activated when post-synaptic depolarizations correlate temporally with glutamate release, thereby sensing and

initiating plasticity related signaling (Cohen & Greenberg, 2008). AMPA receptors, which mediate the majority of excitatory synaptic transmission in the adult CNS (Greer & Greenberg, 2008), have also been noted to be Ca^{2+} permeable and thus important in some developmental systems, although the adult typically expresses only the Ca^{2+} impermeable GluR2 subunit (Cohen & Greenberg, 2008).

Another major source of Ca^{2+} influx arises from voltage-gated Ca^{2+} channels (VGCCs), multi-subunit complexes comprised of the pore-forming α_1 and accessory β, $\alpha_2\delta$ and γ subunits. The α_1 subunits, of which ten have been discovered, contain the binding sites for all known VGCC blockers, the voltage sensor and the selectivity filter, and span the cell membrane six times within each of four domains (Moosmang *et al*., 2005b). The VGCCs are broadly split into two families, the high and low voltage activated channels (HVA and LVA respectively). LVA channels ($Ca_V3.1$-3.3), or T-type for their tiny and transient single-channel currents, do not play much of a function in plasticity. There are seven α_1 HVA channels, broken into P/Q- and N-type ($Ca_V2.1$-2.2, respectively), which function mostly in pre-synaptic vesicle release, R-type ($Ca_V2.3$), which is least known and classically hardest to study because of its drug resistances, and L-type ($Ca_V1.1$-1.4; Dietrich *et al*., 2003). It is becoming increasingly clear that VGCCs, especially the L-type channels, play an important role in neuronal plasticity (Cavazzni *et al*., 2005). L-type Ca^{2+} channels are ideally suited for fluxing large amounts of Ca^{2+} into the cell because of their slow inactivation rate and high single-channel conductance (Greer & Greenberg, 2008). Additionally, they have a relatively low-voltage of activation (–20mV as opposed to 0mV for the Ca_V2 family; Catterall *et al*., 2005) and are typically localized to somatodendritic regions, allowing for the elevation of Ca^{2+} levels in close proximity to the nucleus and enabling efficient signaling. Of the four L-type Ca^{2+} channels, only two are expressed in neuronal tissues, with

$Ca_V1.1$ and 1.4 in cardiac and skeletal muscle, and retina, respectively. $Ca_V1.2$ and 1.3, also known as α_{1C} and α_{1D} respectively, play a major role in the brain as well as in cardiac and skeletal muscle (Moosmang *et al*., 2005b).

While the NMDAR has received the majority of attention, the possible role for L-type Ca^{2+} channels in developmental plasticity has been largely unexplored, although they have been alluded to in a few instances in the super colliculus and brainstem (Lo & Mize, 2000; Guido *et al*., 2001). Additionally, many studies focus on the interplay between channels, such that an initial depolarization mediated by NMDAR is prolonged and augmented by the activation of somatic L-type Ca^{2+} channels (Greer & Greenberg, 2008). Their location, kinetics and high Ca^{2+} fluxes increase the likelihood that the Ca^{2+} signal will reach the cell's nucleus to trigger the transcription of plasticity related genes. However, what seems to be lacking is an examination of L-type Ca^{2+} channels mediating activity-dependent refinement of sensory connections. One such system that has been studied extensively involves the development of retinal projections to the dorsal lateral geniculate nucleus (dLGN) of the thalamus. In the retinogeniculate system, spontaneous retinal activity is needed to drive the segregation of retinal inputs from the two eyes into eye-specific domains in dLGN (Torborg & Feller, 2005; Huberman *et al*., 2008; Guido, 2008). A potential role for L-type mediated activity in the form of so called plateau potentials has been implicated by earlier studies done in the Guido lab (Lo *et al*., 2002; Jaubert-Miazza *et al*., 2005). Plateau potentials, long-lasting, slow decaying depolarizations evoked with high frequency stimulation of retinal ganglion cells, are prevalent at early postnatal ages, during the peak of retinogeniculate refinement. However, many questions remain about the mechanisms that generate these events and their potential role in mediating activity-dependent plasticity. The overall arching goal of my thesis is to address these factors. In the first part of this thesis, we

examine the developmental factors and stimulus conditions that lead to the activation of plateau activity. In the second, we test whether such activity is necessary for the refinement of retinal projections as well as their functional connections onto individual dLGN relay cells. For the latter, a loss-of-function approach has been adopted.

Traditionally, loss-of-function was accomplished either by pharmacological manipulations or visual depravation (Huberman *et al*., 2008). Unfortunately, both are fraught with technical problems that cloud the interpretation of the results; however by simply eliminating specific genes, many of these issues can be rectified. Typically, in such ion channel studies, the pore-forming unit is targeted to completely remove the channel's expression and function. In the case of the L-type Ca^{2+} channel, such an approach is problematic since these channels are also necessary in cardiac and skeletal muscle and $\alpha_{1C}^{-/-}$ mice die before 14.5 days post-conception (Moosmang *et al*., 2005b). Interestingly, conditional $\alpha_{1C}^{-/-}$ mice have been made, in which, using the Cre-loxP site-specific recombination system, the α_{1C} subunit is removed in the hippocampus and neocortex (Moosmang *et al*., 2005a). However, in this mouse the expression of α_{1C} does not appear to be decreased until late postnatal ages (after the 3rd week), making a developmental study infeasible. Additionally, there are no known dLGN specific promoters, further limiting our ability to use a conditional mouse.

Another possible approach involves targeting of one of the subunits of VGCCs that is necessary for membrane trafficking. The β subunit binds to an intracellular portion of the α_1 subunit between the first and second transmembrane domains (Catterall *et al*., 2005). Interestingly, in binding to the α_1, the β subunit seems to obscure an endoplasmic reticulum retention signal and allows for the α_1 to be trafficked to the cell membrane (Dolphin, 2003). There are four β subunits, and although mice lacking the β_1 subunit are not viable (Gregg *et al*.,

1996), the β_3 subunit is not necessary for skeletal or cardiac function as these mice live and breed successfully. Importantly for us, however, they have a greatly reduced neuronal α_{1C} membrane expression (Fig 1.8) and associated L-type current (Namkung *et al*., 1998; Jeon *et al*., 2008). Therefore, we were able to use this mouse to assess whether plateau potential activity, evoked by strong retinal activity during early postnatal development, was necessary for the refinement of retinogeniculate connections in the dLGN.

This thesis is arranged in two related chapters, both of which can be read as separate papers in peer reviewed journals. Chapter 1, entitled "Requirements for synaptically evoked plateau potentials in relay cells of the dLGN of the mouse," is under review at the Journal of Physiology. Chapter 2, entitled "The absence of synaptically evoked plateau potentials in dLGN relay cells leads to a breakdown in retinogeniculate refinement", is a manuscript in preparation.

Chapter 1

Requirements for synaptically evoked plateau potentials in relay cells of the dorsal lateral geniculate nucleus of the mouse

Abstract

In developing cells of the mouse dorsal lateral geniculate nucleus (dLGN), synaptic responses evoked by optic tract (OT) stimulation give rise to long-lasting, high-amplitude depolarizations known as plateau potentials. These events are mediated by L-type Ca^{2+} channels and occur during early postnatal life, a time when retinogeniculate connections are remodeling. To better understand the relationship between L-type activity and dLGN development we used an *in vitro* thalamic slice preparation which preserves the retinal connections and intrinsic circuitry in dLGN and examined how synaptic responses evoked by OT stimulation lead to the activation of plateau potentials. By varying the strength and temporal frequency of OT stimulation we identified at least three factors that contribute to the developmental regulation of plateau activity: the degree of retinal convergence, the temporal pattern of retinal stimulation and the emergence of feed-forward inhibition. Before natural eye opening (postnatal day 14), the

excitatory synaptic responses of relay cells receiving multiple retinal inputs summated in both the spatial and temporal domains to produce depolarizations sufficient to activate L-type activity. After eye opening, when inhibitory responses are fully developed, plateau activity was rarely evoked even with high temporal rates of OT stimulation. When the bulk of this inhibition was blocked by bath application of bicuculline, the incidence of plateau activity increased significantly. We also made use of a transgenic mouse that lacks the β_3 subunit of the L-type Ca^{2+} channel. These mutants have far fewer membrane bound Ca^{2+} channels and attenuated L-type activity. In β_3 nulls, L-type plateau activity was rarely observed even at young ages when plateau activity prevails. Thus, in addition to the changing patterns of synaptic connectivity and retinal activity, the expression of L-type Ca^{2+} channels is a requisite component in the manifestation of plateau activity.

Introduction

Ca^{2+} signaling through L-type Ca^{2+} channels is a prominent feature of many developing neurons and has been implicated in a number of important events including cell survival, axonal and dendritic growth, synaptogenesis and plasticity, as well as intracellular signaling and gene expression (Cohen & Greenburg, 2008; Greer & Greenburg, 2008). L-type channel activation can give rise to diverse patterns of activity, ranging from small spikes, spontaneous membrane oscillations and prolonged firing rates, to large plateau like depolarizations (Rekling & Feldman, 1997; Morisset & Nagy, 1999; Lilelund *et al*., 2000; Singer *et al*., 2001; Lo & Erzurumlu, 2002; Corlew *et al*., 2004; Crepel *et al*., 2007).

In developing neurons of the rodent dorsal lateral geniculate nucleus (dLGN), the excitatory postsynaptic responses evoked by strong or repetitive stimulation of retinal ganglion cell axons are of sufficient strength to activate high threshold L-type Ca^{2+} channels (Lo *et al*., 2002; Jaubert-Miazza *et al*., 2005; Liu & Chen, 2008). This activation gives rise to sustained (~500ms), high amplitude (35-60mV) depolarizations known as plateau potentials. These events are encountered frequently at early postnatal ages but decline with age, so that after natural eye opening (postnatal day (P) 14) plateau activity is rarely observed (Lo *et al*., 2002; Jaubert-Miazza *et al*., 2005). Such timing coincides with a number of important developmental events occurring in the dLGN, including the establishment of segregated retinal projections into eye-specific domains, the pruning of retinal inputs onto dLGN relay cells, and the emergence of feed-forward inhibitory connections (Guido, 2008). Some aspects of this remodeling (e.g., eye-specific segregation) have been attributed to the wave like patterns of spontaneous retinal activity (Torborg & Feller, 2005; Torborg *et al*., 2005; Huberman *et al*., 2008). However, the cellular mechanisms underlying the implementation of these activity-dependent changes remain

largely unknown. Synaptically evoked plateau activity could figure prominently in the remodeling process. L-type Ca^{2+} channel activity has been implicated in long-term changes in synaptic strength of dLGN cells (Ziburkus *et al*., 2009), as well as intracellular signaling cascades involved in the refinement of retinogeniculate projections (Pham *et al*., 2001).

To elucidate the role of plateau potentials, it is important to gain insight into the mechanisms underlying their developmental regulation. The transient nature of these events remains somewhat puzzling. At the time when their incidence is high, individual retinal synaptic events are relatively weak (Chen & Regher, 2000; Hooks & Chen, 2006; Liu & Chen, 2008) and not capable of reaching or sustaining the requisite levels of membrane depolarization necessary to activate L-type channels (Hernandez-Cruz & Pape, 1989; Kammermeier & Jones 1997, 1998). Moreover, by the time that plateau activity wanes, retinal synapses have matured (Bickford *et al*., 2010) and their currents are 7-10 fold larger (Chen & Regehr, 2000; Hooks & Chen, 2006), making them, in principle, sufficient to activate L-type activity. Thus, resolving this issue requires one to examine other aspects of dLGN development. One such element is the changing patterns of synaptic connectivity. Initially, dLGN cells are binocularly innervated, receiving excitatory input from as many as a dozen retinal ganglion cells (Chen & Regehr, 2000; Lo *et al*., 2002; Jaubert-Miazza *et al*., 2005; Hooks & Chen, 2006; Ziburkus & Guido, 2006). Indeed, their coordinated activation by periodic bursts of spontaneous retinal activity can lead to significant levels of membrane depolarization (Mooney *et al*., 1996). In contrast, by P14 many of these inputs have been eliminated, spontaneous retinal waves subside (Demas *et al*., 2003) and the net excitatory drive onto dLGN cells is greatly reduced (Lo *et al*., 2002; Liu & Chen, 2008). In addition to the pruning of excitatory connections, inhibitory circuits that involve GABAeric interneurons of the dLGN emerge, further limiting the degree of postsynaptic membrane

depolarization (Ziburkus *et al*., 2003; Bickford *et al*., 2010). Another important element to consider is the expression of L-type Ca^{2+} channels in the developing dLGN. Based on immunostaining in dLGN, it appears that these channels are heavily expressed at early postnatal ages (Jaubert-Miazza *et al*., 2005) and thus may offer a greater opportunity for the activation of L-type activity at young ages. However, it remains to be tested whether such age related modulation in channel density can affect the incidence of plateau potentials.

To consider how patterns of retinal stimulation as well as the underlying synaptic connectivity of the dLGN contribute to the activation of plateau potentials, we recorded the synaptic responses of developing relay cells in an acute thalamic slice preparation designed to preserve both retinal and intrinsic inhibitory feed-forward connections (Chen & Regher, 2000; Bickford *et al*., 2010). To assess whether L-type Ca^{2+} channel expression is a contributing factor, we made use of a transgenic mouse that lacks the β_3 subunit of the L-type Ca^{2+} channel. These mutants have greatly attenuated L-type activity brought about by improper channel trafficking and kinetics (Birnbaumer *et al*., 1998; Namkung *et al*., 1998; Murakami *et al*., 2002; Shiraiwa *et al*., 2007). Finally, since many of the elements suspected to contribute to the activation of plateau potentials change around the time of natural eye opening (P14), we compared the incidence of plateau activity in dLGN cells before and after P14.

Methods

Ethical approval. All procedures were performed in compliance with the Institutional Animal Care and Use Committee at Virginia Commonwealth University. 50 wild-type C57/BL6 mice and 33 mice of a transgenic strain bred on a C57/BL6 background that lacks the β_3 subunit of the L-type Ca^{2+} channel (Namkung *et al*. 1998) were used. The mice were bred and housed in resident colonies and ranged in age from P7 to 22. *Slice preparation and in vitro electrophysiology*. To examine the synaptic responses evoked by optic tract (OT) stimulation, an acute thalamic slice preparation which preserves retinal and intrinsic inhibitory connections in dLGN was adopted (Chen & Regehr, 2000; Bickford *et al*., 2010). Mice were deeply anesthetized with isoflurane and decapitated. The brain was removed from the skull and immersed into an oxygenated (95% O_2/5% CO_2) 4°C sucrose solution (in mM: 28 $NaHCO_3$, 23 sucrose, 11 $MgSO_4$, 0.11 glucose, 2.75 KCl, 1.4 NaH_2PO_4, 0.5 $CaCl_2$). The two hemispheres were then separated by cutting along the midline at an angle of 10-20°. The medial aspect of the brain was glued onto a tilted (20°) stage of a vibratome (Leica VT1000S) and 300µm sections were cut in the parasagittal plane. Prior to recording, slices were incubated in a holding chamber containing an oxygenated artificial cerebral spinal fluid (ACSF) solution (in mM: 126 NaCl, 26 $NaHCO_3$, 10 glucose, 2.5 KCl, 2 $MgCl_2$, 2 $CaCl_2$, 1.25 NaH_2PO_4) for 30 minutes at 35°C and then brought to room temperature. Individual slices containing the dLGN and a large segment of the optic tract were then transferred to a recording chamber maintained at 32°C, and perfused continuously at a rate of 2.0 ml/min with oxygenated ACSF.

In vitro recordings were done in a whole cell configuration with the aid of a fixed-stage microscope (Nikon E600FN) equipped with differential interference contrast optics and a water-immersion objective to view individual neurons within the slice. Patch electrodes were pulled

vertically in two stages from borosilicate glass and filled with a solution (for current clamp recordings: in mM; 140 K-gluconate, 10 HEPES, 2 MgATP, 0.3 NaCl, 0.1 NaGTP, pH=7.25, 260osmol/L; for voltage clamp recordings: 130 Cs methanesulfonate, 10 HEPES, 10 QX-314, 5 KCl, 5 EGTA, 2 $MgCl_2$, 0.1 CaCl2, 2 MgATP, 0.1 NaGTP, pH=7.25, 260osmol/L). The final tip resistance of filled electrodes was 3-7MΩ. Whole cell recordings were done using an Axoclamp 2B (current clamp) or AM Systems 2400 (voltage clamp) amplifier. Pipette capacitance, series resistance, and whole cell capacitance were carefully monitored and compensated electronically during the recording. Neuronal activity was displayed on an oscilloscope (Hitachi VC-6025A), digitized (10-20KHz) through an interface unit (National Instruments BNC-2090) and stored directly on a computer. Data acquisition and analysis was accomplished by using free software (Strathclyde Electrophysiology Software, Whole Cell Analysis Program V3.8.2.). During some recordings, the GABA antagonists bicuculline (25μM, Tocris 0131) and CGP (10μM, Tocris 1248) were bath applied to block inhibitory activity. Nimodipine (30μM, Tocris 0600) was also bath applied to block L-type Ca^{2+} channel activity.

To evoke synaptic activity in dLGN, square-wave pulses (0.1– 0.3ms, 1-1000μA) were delivered at variable rates of (0.2–100 Hz) through a pair of thin-gauge tungsten wires (0.5MΩ) positioned in the optic tract. The stimulating electrodes were connected to a stimulus isolation unit (World Precision Instruments Stimulus Isolator A360) that received input from a computer controlled, multichannel pulse generator (World Precision Instruments PulseMaster A300) programmed to elicit specific conditioning protocols**.**

Estimates of retinal convergence were accomplished by generating EPSP amplitude by stimulus intensity plots (Fig. 1.3; see also Lo *et al*., 2002; Jaubert-Miazza *et al*., 2005; Ziburkus & Guido, 2006). These were constructed by first determining the minimum stimulus intensity

needed to evoke a postsynaptic response. Once the single fiber response was determined, current intensity was increased in small increments (0.5 to 1.0μA) until a response of maximal amplitude was consistently reached. A minimum of five responses was recorded at each stimulus intensity. A change in amplitude that was equal to or exceeded a value that corresponded to the cell's single fiber response was used to distinguish one input from another. For example, if the single fiber response was 1mV, a value of at least 2mV was needed to delineate the next input; for the subsequent step a value of 3mV was needed. The estimates of retinal convergence obtained in the present study were in accord with those reported previously (Chen & Regehr, 2000; Lo *et al*., 2002; Jaubert-Miazza *et al*., 2005; Hooks & Chen, 2006; Ziburkus & Guido, 2006; Stevens *et al*., 2007).

Immunocytochemistry. To examine the labeling pattern in dLGN for L-type Ca^{2+} channels, slices were processed with either a standard Nissl protocol or incubated with one of two polyclonal rabbit antibodies: one directed toward the pore forming α_{1C} subunit of $Ca_V1.2$ L-type Ca^{2+} channel, and the other toward the accessory β_3 subunit (1:1000, Alomone Labs ACC-003, ACC-008). For tissue preparation, mice were deeply anesthetized with isoflurane and transcardially perfused with phosphate buffer saline (PBS: 0.01mM NaH_2PO_4, 0.9% NaCl, pH 7.4) and 4% paraformaldehyde in 0.1M phosphate buffer. Tissue was post-fixed overnight and sectioned (70μm) in the coronal plane. Sections containing the dLGN were pretreated (30 minutes) in 10% normal goat serum (NGS) in PBS and then incubated in their primary antibody solutions diluted in 1% NGS/PBS overnight at 4°C. The next day, tissue was rinsed in PBS and incubated at room temperature (1 hour) in 1% NGS/PBS solution containing a biotinylated goat anti-rabbit (1:400, Sigma B8895) secondary antibody. Following a series of buffer rinses, tissue was incubated (1 hour) in an avidin and biotinylated horseradish peroxidase (1:100, Vector Labs

B-2004) 1% NGS/PBS solution. Sections were then reacted with a nickel intensified diaminobenzidine (DAB) solution (1–2 minutes), washed in sodium acetate, mounted on slides, dehydrated, and cover slipped for light microscopy. Digital images of labeled cells were acquired with a Kodak CD 290 camera mounted on the head of a Nikon Labophot light microscope. Cell density measurements were carried out as reported previously (Jaubert-Miazza *et al*., 2005). Labeled cells were included if their nucleus or a continuous cell membrane was readily discerned in a given focal plane. Cell density measurements were computed by counting labeled cells in a 100μm^2 area within the centre of dLGN in two sections of five separate mice. These sections were also used to obtain maximal length and width measurements of dLGN.

Western Blots. To examine protein expression of L-type Ca^{2+} channels, mice were deeply anesthetized with isoflurane and decapitated. The brain was removed from the skull and immersed into an oxygenated 4°C saline solution (in mM: 126 NaCl, 10 glucose, 2.5 KCl, 2 $MgCl_2$, $2CaCl_2$, 1.25 NaH_2PO_4). The dLGN from both hemispheres was dissected from 400µm thick coronal sections. Tissue was placed in a sucrose buffer (320mM with 2% Complete Protease Inhibitor, Roche Diagnostics 11836153001) and stored at –80°C. Each sample contained dLGNs from 4 mice. Tissue was defrosted on ice, homogenized in sucrose buffer and the total protein concentration was determined using the Quick Start Bradford protein assay kit (Bio-Rad 500-0207). 30µg of protein from each sample was loaded onto a Criterion 10% or gradient 4-20% Tris-HCl polyacrylamide gel (Bio-Rad 345-0009 and -0032 respectively). The protein was transferred overnight at 4°C to a nitrocellulose membrane (Bio-Rad 162-0115). Membranes were blocked with 5% powdered milk in Tris-buffered saline with Tween 20 (TBST, 1 hour), then incubated (1.5 hour) with antibodies directed towards various subunits of the L-type Ca^{2+} channel: α_{1C}, α_{1D}, β_3 (1:200, Alomone Labs AAC-003, -005 and -008, respectively),

β_{1b}, β_2 and β_4 (1:250, a generous gift from Kevin Campbell) in 5% BSA in TBST. GAPDH (1:100,000; Cell Signaling 2118) was used as a loading control. The membranes were washed with Tris-buffered saline and treated with the secondary antibody, peroxidase goat anti-rabbit (1:10,000, Jackson ImmunoResearch 111-035-003), in TBST (1.5 hour) at room temperature. SuperSignal West Pico chemiluminescent detection reagent (Pierce 34077) was used to visualize immunoreactivity. Analysis was performed using Kodak 1D Image Analysis Software.

Results

We studied the synaptic responses evoked by OT stimulation for 152 dLGN cells in mice that were 7-22 days old. Of these, 101 were recorded from wild-type (WT) and 51 from transgenic mice lacking the β_3 subunit of the L-type Ca^{2+} channel. For Figures 1.3-1.7, 1.10 and Table 1, cells are divided into two age groups: before P14 (P7-13) and after P14 (P14-22). All cells had resting membrane levels between –56 and –68mV, an input resistance of $\geq$200MΩ and overshooting action potentials. Measurements of time constants of cells recorded before and after P14 were also similar (Table 1).

Figure 1.1 illustrates the basic features of synaptically evoked plateau potentials in dLGN (see also Lo *et al*., 2002; Jaubert-Miazza *et al*., 2005). These events, which prevail at early postnatal ages, are defined as long lasting (100-500ms), high amplitude (35-60mV), slow decaying depolarizations. Riding the crest of this response is a train of action potentials of variable amplitude and duration. Plateau potentials can be activated when the OT is stimulated with single (Fig. 1.1A, *left*) or repetitive pulses (Fig. 1.1B-D, *left*). They are mediated by the voltage-dependent activation of high threshold L-type Ca^{2+} channels. Bath application (n=7 cells) of L-type Ca^{2+} channel antagonists such as nimodipine (Fig. 1.1A-B, *right*) block the activation of plateau potentials while leaving the underlying synaptic events intact. At resting levels (e.g., –60 mV Fig. 1.1C, *left*), EPSP activity provides an adequate amount of depolarization to activate plateau activity; however, when hyperpolarized (e.g., –95 mV, Fig. 1.1C, *right top*) by DC current injection, these events are no longer sufficient for L-type activation. In fact, when nimodipine is applied at these hyperpolarized levels, (Fig. 1.1C, *right bottom*) postsynaptic activity remains unaffected. Additionally, in some instances at young postnatal ages, nimodipine-sensitive plateau-like depolarizations could be evoked by

depolarizing current injection (5 of 35 cells, 14%; Fig. 1.1D; also see MacLeod *et al*., 1997). Finally, neither NMDA mediated activity nor intracellular Ca^{2+} release contribute to these events, since plateau potentials persist and remain relatively unaltered after the application of the NMDA antagonist APV (n=6 cells; Fig. 1.2A), or the internal use of the Ca^{2+} chelator BAPTA (n=5 cells; Fig. 1.2B).

Figures 1.3 and 1.4 highlight how the sustained depolarization associated with the spatial and temporal summation of retinally evoked EPSPs leads to the activation of plateau potentials. To illustrate the effects of spatial summation, responses to a single shock of varying stimulus intensity were used (Fig. 1.3). At young ages (P11, Fig. 1.3A, *left*), a progressive increase in stimulus intensity led to graded increases in EPSP amplitude that eventually gave rise to a plateau potential. By contrast, at late ages (P22, Fig. 1.3A, *right*) this protocol produced a few step-like changes in EPSP amplitude, but, rather than a plateau potential, a single Na^{+} spike emerged. Whether graded or step-like, these increases in EPSP amplitude brought about by increasing stimulus intensity are taken to reflect the recruitment of multiple retinal inputs converging onto a single dLGN cell (Chen & Regehr, 2000; Jaubert-Miazza *et al*., 2005; Hooks & Chen, 2006). The corresponding EPSP amplitude by stimulus intensity plots can then be used to obtain estimates of retinal convergence (see methods for details). The plots in Figure 1.3 reveal that a cell recorded at P11 had at least 8 retinal inputs whereas in a P22 cell only 2 were observed. Because dLGN cells tend to receive far more retinal inputs prior to eye opening (Chen & Regehr, 2000; Jaubert-Miazza *et al*., 2005; Hooks & Chen, 2006), their summation and resulting depolarization should increase the likelihood of generating a plateau potential. In fact, as shown in Figure 1.3B, before the time of natural eye opening (before P14), a single high

intensity stimulus evoked a plateau in 18 of 38 cells (47%). However, after P14, none of the 24 cells tested exhibited plateau activity (χ^2 test: $p<0.0001$).

A similar age-related pattern emerged when EPSPs summate in the temporal domain. To illustrate the effects of temporal summation, responses to repetitive stimuli varying in temporal frequency (5, 10, 20, 50, 100 Hz) were used (Fig. 1.4A). For these recordings, stimulus intensity was held constant at a value that yielded an EPSP of half maximal amplitude. At all ages, increasing temporal frequency led to an increase in the incidence of plateau potentials. However, at young ages (P10, *top*), plateau potentials could be evoked even at relatively low temporal frequencies (e.g., 10 Hz). By contrast, at older ages (P15, *center*) higher temporal frequencies were needed to evoke plateaus, and for many cells (P22, *bottom*) they became difficult to evoke even at the highest temporal frequency tested (100Hz). These effects are summarized in Figure 1.4B, which plots the incidence of plateau potentials as a function of temporal frequency. The incidence of plateau potentials evoked by repetitive stimulation was significantly higher before (21 of 31 cells, 68%) than after P14 (3 of 24 cells, 13%; χ^2 test: $p<0.0001$). Moreover, before P14, within single cells, the incidence of plateau potentials increased as a function of temporal frequency, from 10% at 5Hz to over 60% at 20, 50 and 100Hz. Conversely, after P14, repetitive stimulation failed to evoke plateau potentials at frequencies up to 20Hz, and, even at 100Hz, plateaus were rarely observed (13%). Such efficacy at low rates of stimulation can in part be attributed to the long decay time of the NMDA mediated component of the EPSP (Scharfman *et al*., 1990; Lo *et al*., 2002), which is best illustrated in the responses evoked using 50Hz stimulus (Fig. 1.4A). In order to fully consider these effects, we conducted voltage clamp recordings at +40mV to observe the outward currents of NMDA receptors (NMDAR). Consistent with previous reports, relay cells recorded before P14 showed significantly slower decay times (Fig.

1.4C; 144.0 ± 5.6ms) compared to cells recorded after P14 (96.7 ± 10.1ms, one way ANOVA: $p<0.0001$). As a result, the depolarization from EPSPs recorded at younger ages is prolonged, thereby increasing the likelihood that subsequent stimuli will more readily lead to L-type activation.

Taken together, these results suggest that the spatial and temporal summation of EPSPs contribute to the activation of plateau potentials, and that these events are far more likely to occur at early postnatal ages when dLGN cells exhibit a high degree of retinal convergence. When this relationship was assessed directly for a group of 30 cells (Fig. 1.5), those with five or more retinal inputs, 87% (13 of 15 cells) exhibited a plateau potential, all of which were from young postnatal mice (before P14). By contrast, 80% (12 of 15) of cells with 1-4 inputs failed to display a plateau potential, 9 of which were from late postnatal mice (after P14).

Another factor that can regulate the degree of postsynaptic depolarization is the inhibitory activity arising from feed-forward connections between intrinsic interneurons and relay cells (Crunelli *et al*., 1988; Ziburkus *et al*., 2003; Blitz & Regehr, 2005). At late postnatal ages (after P14), OT stimulation often evokes an EPSP followed by IPSP activity (Bickford *et al*., 2010). As shown in Figure 1.6A, inhibitory responses typically contain two hyperpolarizing components, an early, short-duration IPSP that is blocked by the $GABA_A$ antagonist bicuculline and a slower, long-duration IPSP that is blocked by the $GABA_B$ antagonist CGP. Here, we studied how the emergence of the predominant form of inhibition, the $GABA_A$ mediated IPSP, affects the activation of plateau potentials. After P14, OT stimulation with either a single (Fig. 1.6B, *right*) or repetitive (Fig. 1.6C, *right*) pulses evoked IPSP activity. The inhibitory response limits the amplitude and duration of the preceding EPSP and the cell fails to activate plateau activity. However, when bicuculline is applied and $GABA_A$ inhibition eliminated, the same form of

stimulation led to a plateau potential (Fig. 1.6B-C, *left*; n=7). These effects are summarized in Figure 1.6D-E which plot the incidence of plateau potentials recorded in the presence of bicuculline at ages before and after P14. Before P14, the incidence of plateau potentials evoked by single (13 of 26 cells, 50%) or repetitive stimulation (21 of 26 cells, 81%) was similar to those recorded in control ACSF (Fig. 1.3B, single pulse 47%; Fig. 1.4B, repetitive pulses 68%). However after P14, bicuculline application led to a significant increase in the incidence of plateau potentials for both single (Fig. 1.6D; bicuculline 2 of 20 cells, 10% vs. Fig. 1.3B, control ACSF 0%; χ^2 test: $p<0.01$) and repetitive (Fig. 1.6E; bicuculline 8 of 23 cells, 35%; vs. Fig. 1.4B, control ACSF 13%; χ^2 test: $p<0.001$) forms of stimulation. However, this increase observed at older ages did not approach levels recorded before P14 (χ^2 tests: single and repetitive pulses: $p<0.0001$).

To examine the age related decrease in the expression of the L-type Ca^{2+} channel reported by others (Jaubert-Miazza *et al*., 2005), we performed western blot analysis in homogenized dLGN using antibodies directed to two pore forming subunits, α_{1C} (240kDa), α_{1D} (255kDa) and the ancillary β_3 (55kDa) of the L-type Ca^{2+} channel (Fig. 1.7). After P14 (n=6) the protein expression level of these subunits fall to about 35-40% compared to values obtained before P14 (n=6). Whether this age related decrease has a direct impact on the incidence of plateau potentials has not been explored. To address this, we made use of a mutant mouse in which the structural and functional features of L-type Ca^{2+} channels are disrupted, leading to greatly reduced L-type currents (Namkung *et al*., 1998). This was accomplished by the targeted deletion of the β_3 accessory subunit, an element that is critical for proper channel kinetics, assembly and membrane insertion (Dolphin, 2003). In order to assess L-type Ca^{2+} channel expression in β_3 null mice, we performed immunocytochemistry and western blot analysis in

dLGN (Fig. 1.8). In WT mice, both β_3 and α_{1C} labeling was evenly distributed throughout dLGN. High-power views of dLGN labeled cells also confirmed that staining was confined largely to the somata and proximal dendrites. To best illustrate the stark contrast in β_3 staining between WT and β_3 null mice, Fig. 1.8A presents the labeling pattern in a P28 WT, which has a relatively low density of staining compared to younger WT mice, to that of a P7 β_3 null. As expected in β_3 null mice, β_3 labeling was completely absent. In addition, the staining for α_{1C} was severely reduced in the β_3 null (Fig. 1.8B). At P7 there was a 60% reduction in the density of labeled dLGN cells compared to age matched WT mice (Fig. 1.8C, n=5 WT, mean=25 cells/100μm^2 vs. n=5 β_3 null, mean=10 cells/100μm^2; Student's t-test: $p<0.0001$). Western blots (Fig. 1.8D) of dLGN from WT (n=4) and β_3 null (n=5) mice at P10 showed a similar pattern. WT tissue exhibited strong expression of α_{1C}, α_{1D} and β_3 whereas in β_3 nulls, the expression of α_{1C} and α_{1D} was greatly reduced and β_3 was absent. When α_{1C} protein levels were quantified against a GAPDH loading control, β_3 nulls exhibited a 64% reduction compared to WT (Fig. 1.8E). Furthermore, when the rest of the β subunits (β_{1b} [57.9kDa], β_2 [68.2kDa] and β_4 [58.0kDa]) were analyzed, the protein levels were similar to those in WT (Fig. 1.8D), indicating that they not show any form of compensation in response to the loss of β_3.

While β_3 null mice show a highly reduced expression of L-type Ca^{2+} channels, the structural composition of dLGN was indistinguishable from WT. For example, as shown in Fig. 1.9A, Nissl stains did not reveal any gross abnormalities in the cytoarchitecture of dLGN and adjacent thalamic nuclei. In addition, cell density measurements and the overall size of dLGN were similar in WT (n=5 mice) and β_3 nulls (n=5 mice, Fig. 1.9B). Thus, these observations are consistent with other reports showing that the structural and functional composition of a number

of identified central structures, including the retina is largely similar to WT (Ball *et al*., 2002; Shiraiwa *et al*., 2007; Jeon *et al*., 2008).

The reduced expression of the α_{1C} subunit in β_3 null mice had a direct consequence on the incidence of plateau activity. Synaptically evoked plateau potentials in β_3 nulls were rarely observed (Fig. 1.10B-C). A single shock delivered to OT was never able to evoke plateau activity even at early ages or when high levels of stimulation were used (before P14, 0 of 26 cells; after P14, 0 of 24 cells). When repetitive stimulation was used, the encounter rate of plateau activity for 26 cells recorded before P14 was only 8% for 50Hz and 38% for 100Hz stimuli compared to values of 68% for WT (Fig. 1.4B, χ^2 tests: 50 and 100Hz: $p<0.0001$). For cells recorded after P14, the incidence of plateau potentials evoked by maximal repetitive stimulation was only 4%. These losses are not likely due to any functional abnormalities since dLGN cells from β_3 nulls possess many of the membrane properties and synaptic responses found in WT (Table 1, Fig. 1.11). The voltage responses to intracellular current injection revealed similar patterns of rectification. Additionally, β_3 null cells possessed a mixed cation conductance (H) that gave rise to strong inward rectification and depolarizing sag, rebound low threshold Ca^{2+} spikes (LT) and burst firing (B), an outward rectification that resulted in a delay in spike firing (A) and spike frequency accommodation (afterhyperpolarization, AHP). Synaptic responses evoked by OT stimulation were also similar to WT and were comprised of EPSPs followed by IPSP activity (Fig. 1.10A). The decay times of NMDAR in β_3 nulls was similar to age-matched WTs (τ: before P14: 145.5±3.6, n=37 cells; after P14: 87.4±4.9, n=35 cells; see Fig. 1.4C for WTs), as was the incidence of IPSP activity (P7-11: 16%; P12-15: 48%; P16-20: 79%; P20+: 94%; see Bickford *et al*., 2010 for WTs).

Figure 1.1

Features of synaptically evoked plateau potentials in developing dLGN cells: spatial and temporal summation and voltage dependency.

A. Synaptic responses of a P12 dLGN cell triggered by a single electrical pulse (300μA) delivered to the optic tract (OT) in normal ACSF (*left*) and then after bath application of the L-type Ca^{2+} channel antagonist nimodipine (*right*). In normal ACSF, OT stimulation evokes a plateau potential, characterized as a fast rising, high-amplitude (≥35mV) sustained depolarization (~500ms) that has a burst of inactivating sodium spikes riding its crest. Bath perfusion of nimodipine blocks the plateau potential but leaves the underlying EPSP intact. *B*. Synaptic responses at P14 evoked by repetitive stimulation (5 pulses at 20Hz), before (*left*) and after bath applied nimodipine (*right*). In normal ACSF, repetitive stimulation evokes a large and sustained plateau potential. Bath perfusion of nimodipine blocks the plateau potential, leaving the summating EPSPs intact. Responses in *A*-*B* recorded at –60mV. *C*. Synaptic responses at P9 evoked by repetitive OT stimulation (5 pulses at 20Hz) at –60mV (*left*) and –95 mV (*right top*), and in the presence of nimodipine (*right bottom*). Membrane levels were controlled by injecting DC current through the recording electrode. At the relatively depolarized level of –60mv, the temporal summation of EPSPs gives rise to a plateau potential. At the more hyperpolarized level of –95mV, the same form of stimulation produces a large postsynaptic response but fails to activate L-type channels and evoke a plateau potential. Application of nimodipine reveals that L-type channels are not active in this response. *D*. Injection of 0.1nA current for 200ms can evoke a plateau potential at young ages (P9, *left*) and nimodipine reduces this response to Na^{+} spikes (*right*).

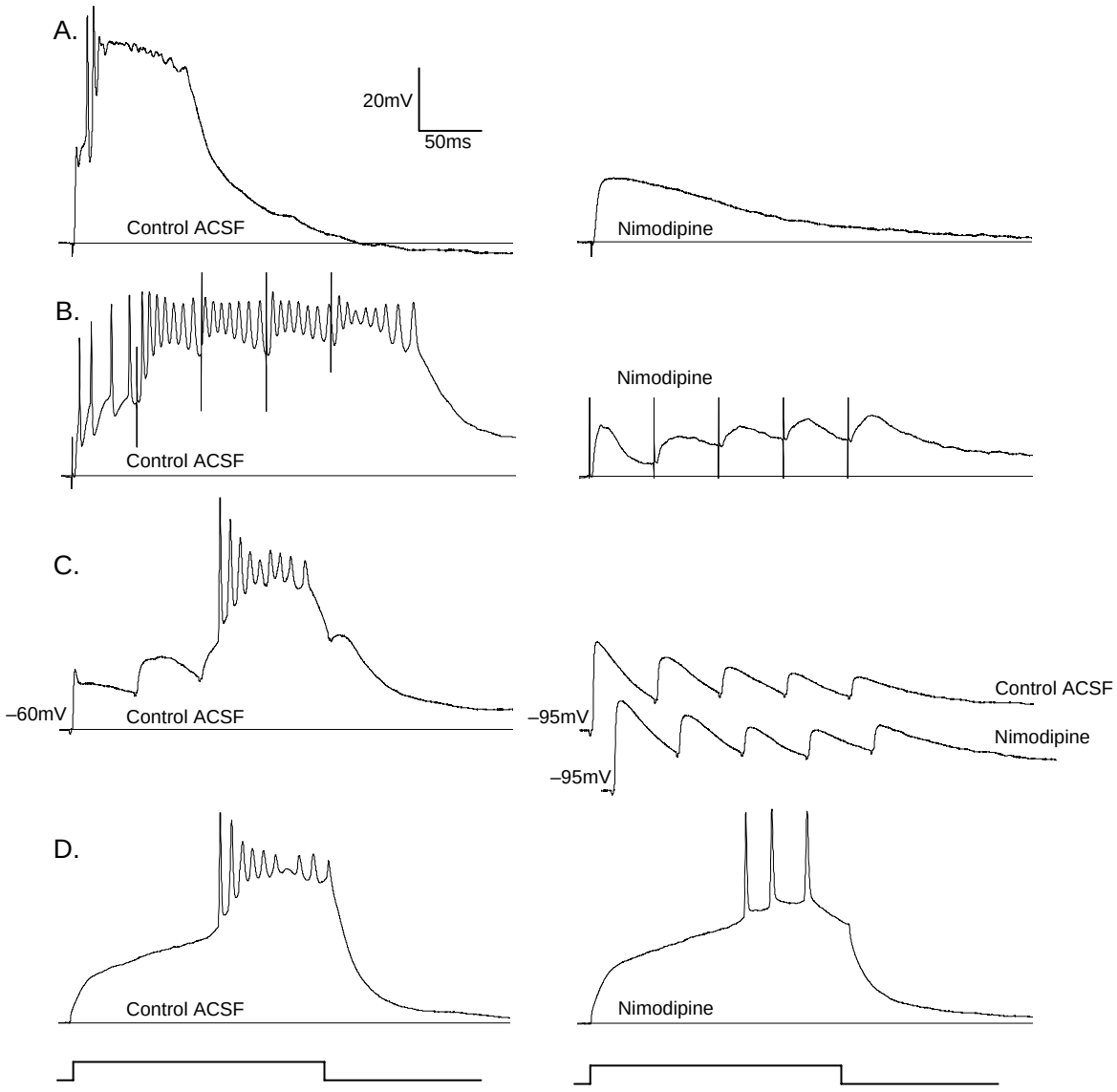

Figure 1.2

Features of synaptically evoked plateau potentials in developing dLGN cells: pharmacology

A. Responses at P14 evoked by repetitive stimulation (5 pulses at 50Hz), before (*left*) and after bath application of the NMDAR antagonist APV (*right*). The plateau potential is not affected. *B.* Response at P8 evoked by 5 pulses at 50Hz with the Ca^{2+} chelator BAPTA in internal solution. Plateau potentials can still be evoked. Responses in *A-B* recorded at –60mV.

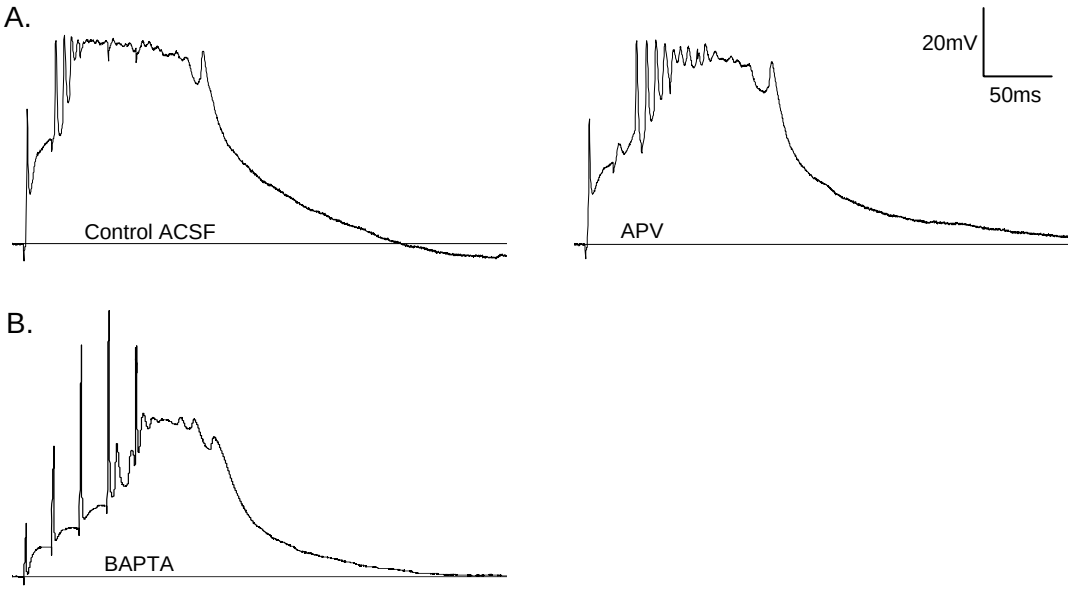

Figure 1.3

Factors that regulate the incidence of plateau potentials in developing dLGN cells: retinal convergence and spatial summation.

A. Examples of synaptic responses evoked by progressive increases in the stimulus intensity of OT stimulation at P12 (*left*) and P22 (*right*) dLGN cells, with the first response magnified for clarity. Beneath each group of responses is the corresponding amplitude by stimulus intensity plots. At P12, a systematic increase in stimulus intensity (*superimposed traces*) leads to graded increases in EPSP amplitude. High levels of OT stimulation lead to the spatial summation of multiple inputs and the generation of a plateau potential (*top most trace*). At P22, the same stimulus protocol evokes a step-like increase in EPSP amplitude that gives rise to an EPSP with a Na^+ spike riding its peak. For EPSP amplitude by stimulus intensity plots, each point depicts the peak amplitude of a single response. A minimum of five responses are recorded at each stimulus intensity. The horizontal lines reflect the calculated threshold between separate retinal inputs (see Methods). Estimated number of inputs at P11 is 8 and 2 at P22. Responses recorded at –60mV in normal ACSF. *B.* Plot showing the incidence of plateau potentials encountered before and after P14. The incidence of plateaus was higher before P14 when developing dLGN cells tend to receive multiple retinal inputs.

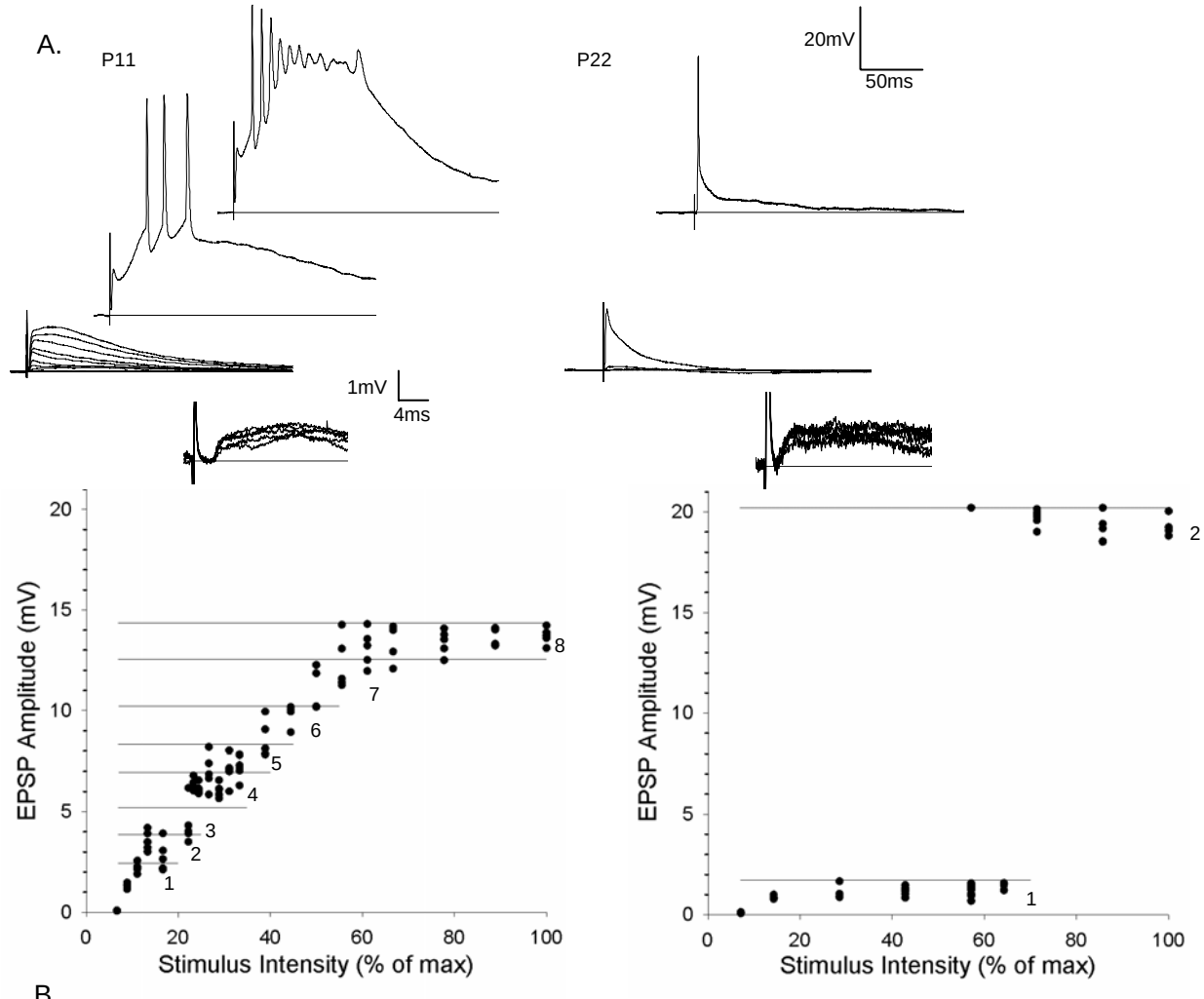

Figure 1.4

Factors that regulate the incidence of plateau potentials in developing dLGN cells: temporal summation.

A. Examples of synaptic responses evoked by 5 pulses of repetitive (5Hz, 10Hz, 20Hz, 50Hz) OT stimulation at three different postnatal ages (P10, P15, P22). At P10, plateau potentials are evoked when stimuli as low as 10Hz are used, whereas at P15, 20 Hz is needed, and at P22 even a 50Hz train could not activate a plateau potential. Responses recorded at –60mV in normal ACSF. ***B*.** Plot showing the percentage of cells that exhibited a plateau potential as a function of temporal frequency, before (filled circles) and after P14 (open circles). Each cell was tested at 5, 10, 20, 50 and 100Hz. Before P14, the incidence of plateau potentials was higher at all temporal frequencies. *C*. Representative NMDAR current traces at P10 and P16 (*right*). Traces are normalized to peak current to highlight changes in decay time. τ values were determined with a single exponential fit (0 to 500ms) while holding cells at +40mV (Hooks & Chen, 2006). Plot showing mean and S.E.M. decay τ values (ms) before and after P14 (*left*). Decay times are slower before P14 than after.

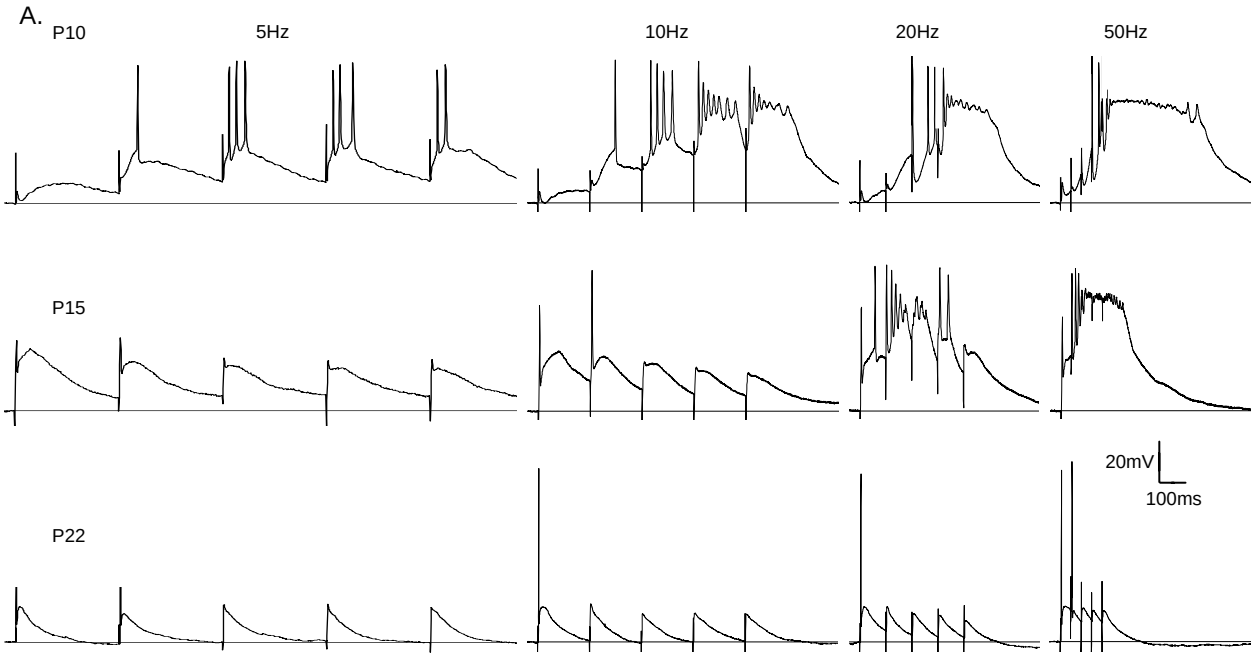

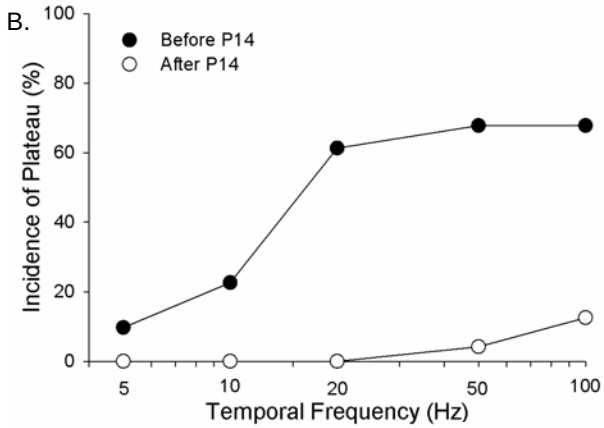

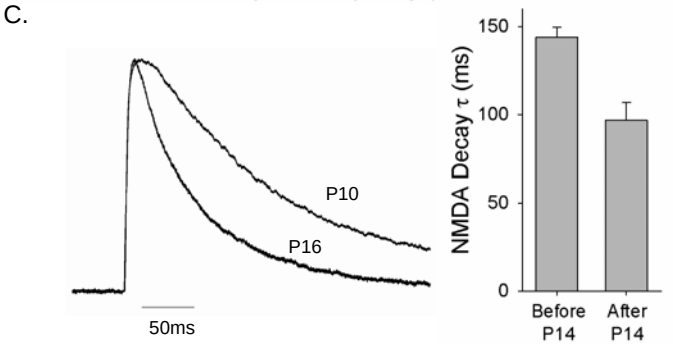

Figure 1.5

Relationship between postnatal age, degree of retinal convergence, and incidence of plateau potentials.

Cumulative frequency plot showing the estimated number of inputs for a given dLGN cell. Each point represents a single cell. Large circles and the dashed line delineate cells that exhibited plateau potentials (PP) with single or repetitive stimulation, whereas small circles and the solid line depict cells in which plateau activity was absent. Filled and open symbols specify cells that were recorded before and after P14, respectively. Plateau potentials tended to occur before P14 and in cells that receive more than 4 inputs.

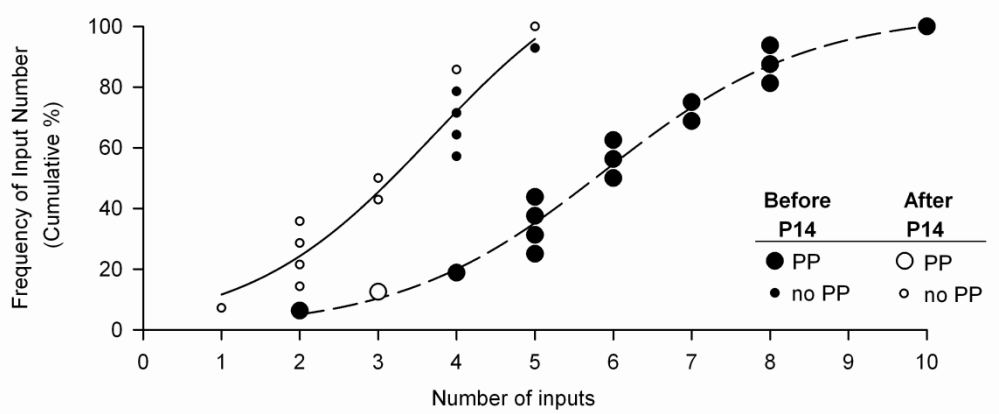

Figure 1.6

Factors that regulate the incidence of plateau potentials in developing dLGN cells: feed forward inhibition.

A. Example of synaptic response recorded at P13 before (control ACSF, *left*) and after the bath application of the $GABA_A$ antagonist bicuculline (*center*), and the $GABA_B$ antagonist CGP (*right*). In control ACSF, the synaptic response contains an EPSP followed by IPSP activity that has two components, an early fast one ($GABA_A$) followed by a slower, longer one ($GABA_B$). Bicuculline blocks the early IPSP and increases the size and duration of the preceding EPSP. CGP eliminates the late IPSP and further increases the amplitude and duration of the EPSP. *B.* Example of synaptic responses recorded at P14 before (control ACSF, *left*) and after bath application of bicuculline (25μM, *right*). In control ACSF, a single electrical pulse applied to OT generates a postsynaptic response that has a Na^+ spike riding the peak of the EPSP/IPSP pair. With the addition of bicuculline, OT stimulation leads to a plateau potential. *C.* Example of another cell's response at P14 before (control ACSF, *left*) and after the bath application of bicuculline (25μM, *right*). A train of 3 pulses delivered at 20Hz evokes a complex response that contains a Na^+ spike and EPSP and IPSP activity. Again, the addition of bicuculline gives rise to a plateau potential. Responses in *A-C* recorded at –60mV. *D.* Plot showing the incidence of plateau activity evoked by single OT stimulation in the presence of bicuculline, before and after P14. *E.* Similar plot showing plateau activity evoked by repetitive OT stimulation in bicuculline (Bic), before (closed circles) and after (open circles) P14. For comparison, the incidence of plateau potentials in control ACSF is plotted in grey (Ctr, as in Fig. 1.4B). After P14 bicuculline led to an increase in the incidence of plateau activity.

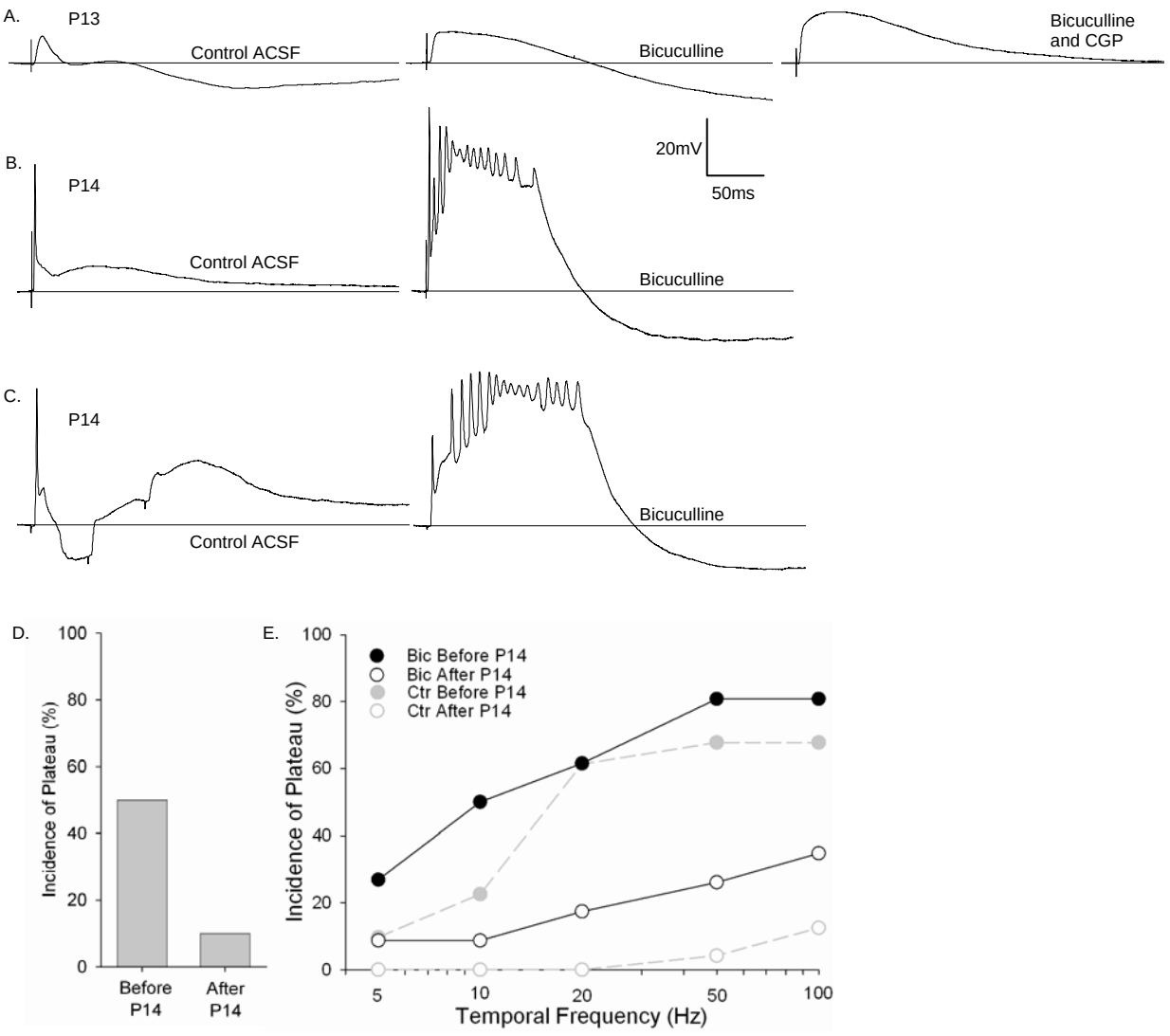

Figure 1.7

Factors that regulate the incidence of plateau potentials in developing dLGN cells: L-type Ca^{2+} channel expression.

Western blots of dLGN tissue before and after P14 using antibodies for the pore forming α_{1C} and α_{1D} subunits as well as the β_3 accessory subunit, using GAPDH as a loading control (*left*). *Right*, a plot of the change in density measurements of each subunit with age, expressed as percentage of before P14. There is a developmental decrease (35-40%) in the expression of all three subunits with age.

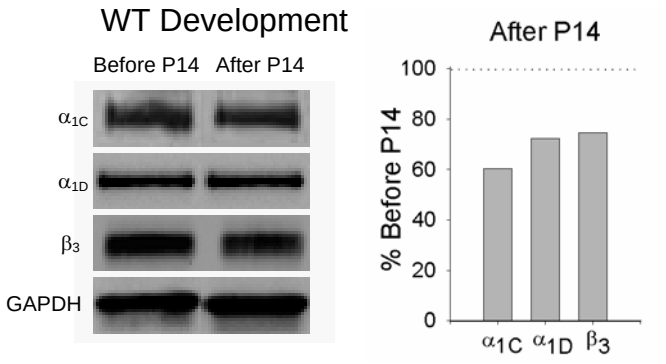

Figure 1.8

Immunocytochemistry and western blot analysis of L-type Ca^{2+} channel subunits in WT and β_3 null dLGN.

A-C. Representative coronal sections in dLGN showing the cellular labeling pattern obtained with antibodies directed toward the ancillary β_3 (*A*; P28 WT, P7 β_3 null) or the pore forming α_{1C} subunit (*B*; P7 WT and β_3 null) in WT and β_3 null mice. Mean and S.E.M. of density of cells labeled for α_{1C} at P7 in WT (n=5) and β_3 null (n=5) mice (*C*). β_3 nulls show an absence of β_3 labeling and a 60% reduction in the density of cellular labeling for α_{1C}. High power images from sections shown above, images acquired with same exposure times. Scale bar: low power - 100μm; high power - 25μm. *D-E*. Western blots of P10 dLGN tissue using the same antibodies in addition to ones for the pore forming α_{1D} subunit and the alternative β subunits (β_{1b}, β_2 and β_4). An antibody directed toward GAPDH was used as a loading control. Plot showing density measurements of L-type Ca^{2+} channel subunit protein levels, expressed as a percentage of WT. In β_3 nulls, α_{1C} showed a 70% reduction and α_{1D} a 40% reduction when compared with WT, β_3 expression was absent, and the expression of the other β subunits was similar to WT.

A.

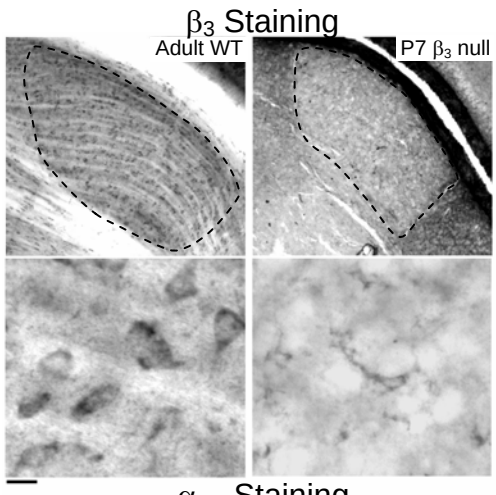

B.

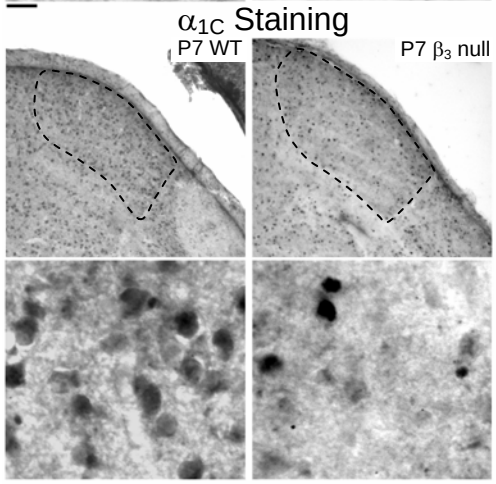

C.

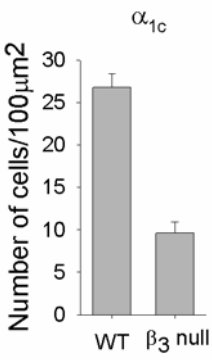

D.

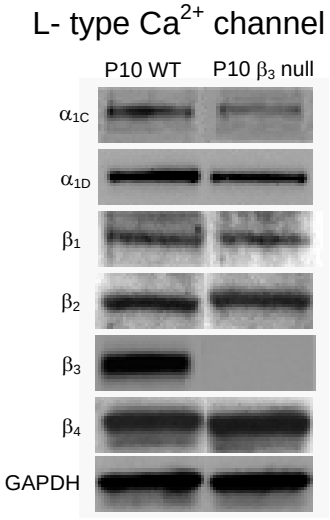

E.

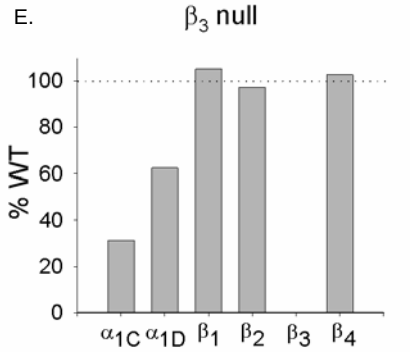

Figure 1.9

Cytoarchitecture of dLGN and surrounding nuclei in WT and β_3 nulls.

A. Representative coronal sections through dLGN showing Nissl stained cells in WT (*left*) and β_3 null mice (*right*). Magnified images (100μm^2) taken from indicated area inset. Outlines indicate borders of dLGN and VLG. Cytoarchitecture of β_3 null dLGN is similar to WT. Scale bar: low power - 100μm; high power - 25μm. *B*. Plots showing cell counts (*left*) and measurements of dLGN length and width (*right*) reveal no abnormalities in β_3 nulls (grey) as compared to WT (black).

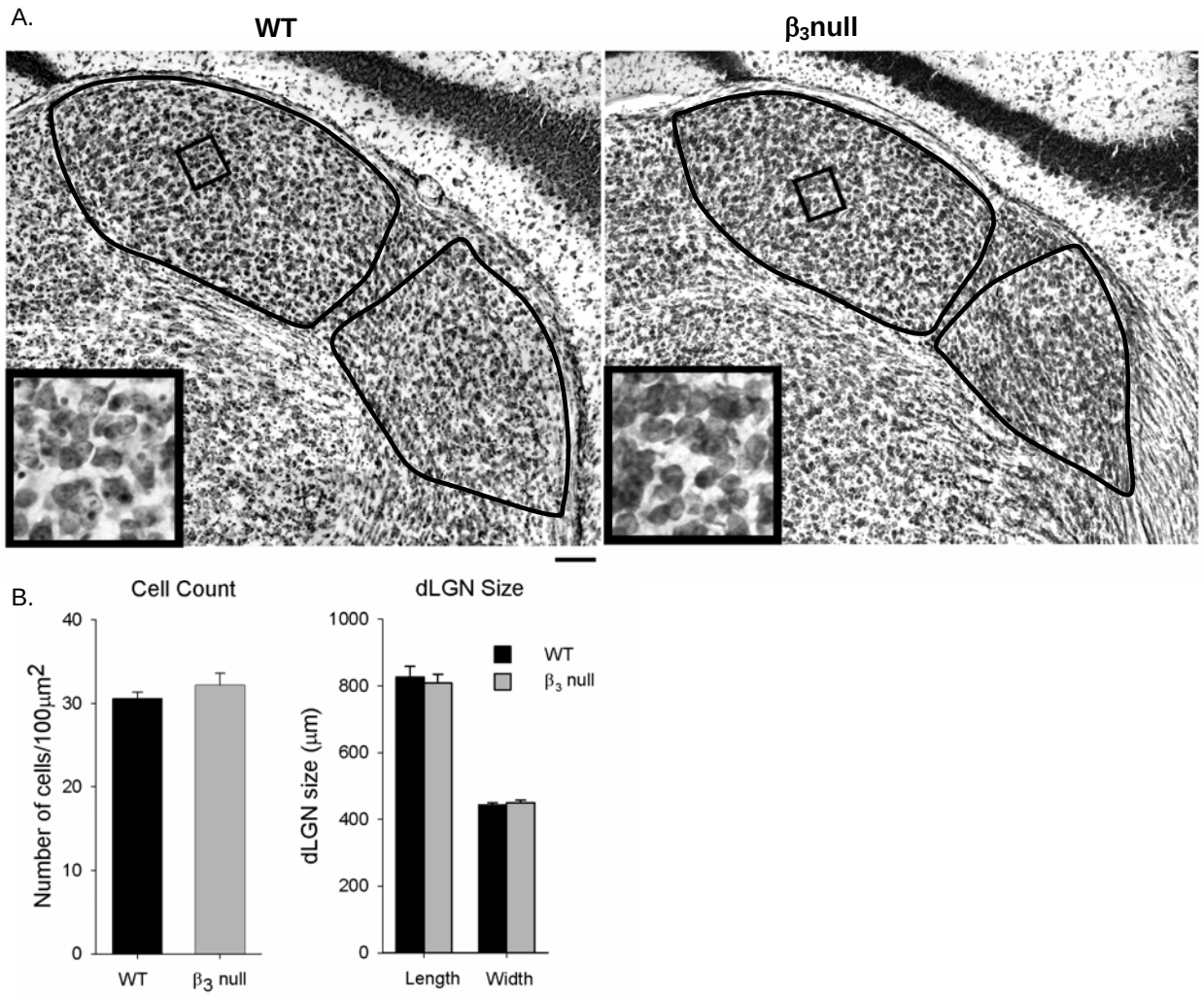

Figure 1.10

Electrophysiological composition of dLGN in WT and β_3 nulls.

A-C. Examples of synaptic responses evoked by OT stimulation at different postnatal ages for WT and β_3 null dLGN cells. *A*. Single pulse OT stimulation (WT P15, β_3 null P18) evokes EPSPs followed by IPSP activity. *B*. At early postnatal ages (WT P11 and P12, β_3 nulls P8 and P10), a single pulse (*top*) or a train of 5 at 100Hz (*bottom*) readily evokes plateau activity in WT (*left*). In β_3 nulls (*right*), plateau activity is rare. Responses in *A-B* recorded at –60mV in normal ACSF. *C*. Plot showing the percentage of cells that exhibited a plateau potential as a function of temporal frequency, before (filled circles) and after P14 (open circles) for cells recorded in β_3 null mice. Overall, the incidence of plateau activity was rare even before P14 and when high rates of stimulation were used.

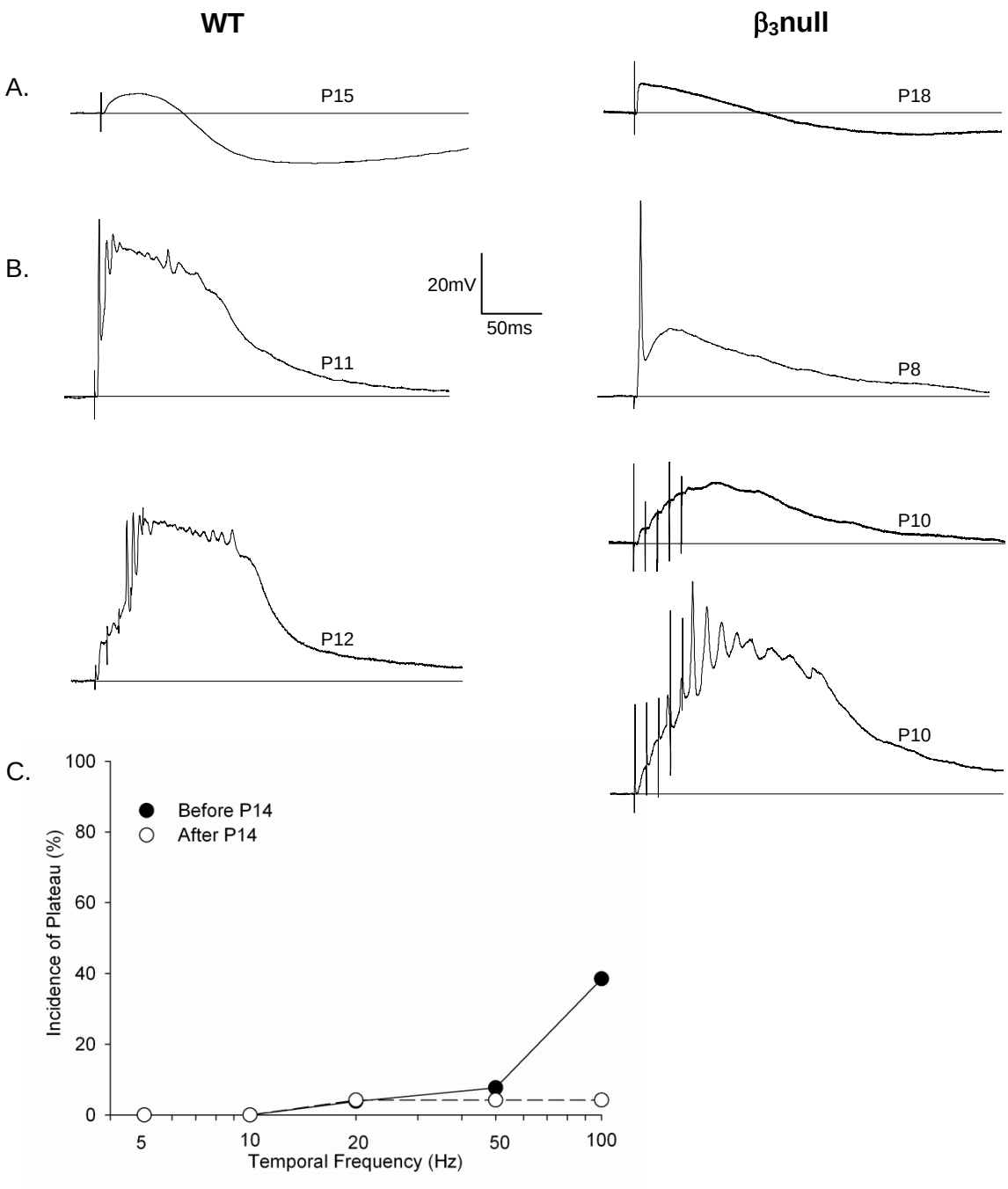

Table 1. Intrinsic Membrane Properties

Property	WT	β_3 null
Time Constant (ms)*		
Before P14	47.5 ± 2.5 (24)	50.5 ± 3.4 (24)
After P14	43.1 ± 3.0 (28)	43.7 ± 3.3 (25)
Input resistance	343.5 ± 25.9 (59)	339.4 ± 27.3 (54)
Low Threshold Ca^{2+} spike	93.8% (64)	95.2% (63)
Low Threshold Ca^{2+} burst	41.4% (58)	48.3% (58)
Mixed cation conductance	82.3% (62)	74.1% (58)
A-type K^+ conductance	91.2% (57)	88.4% (43)

The mean ± SEM or percent incidence for each property are shown, number of cells are shown in parenthesis. Statistical analysis of the mean differences between WT and β_3 null for each property was calculated using a Student's t-test. None of the values are statistically different. Statistical analysis of the percent incidence between WT and β_3 null for each property was calculated using a χ^2 test. None of the values are statistically different.
*We were able to fit 90% to a single exponential curve.

Figure 1.11

Membrane properties of WT and β_3 null relay cells.

A. Examples of voltage responses to current pulse injections from dLGN cells recorded in WT and β_3 null mice. In both strains, a number of active membrane properties were present. Membrane hyperpolarization (-0.1nA) activates a mixed cation conductance (H) and produces an inward rectification. Termination of the hyperpolarizing current pulse leads to the activation of low threshold Ca^{2+} conductance (LT) and burst response (B). Membrane depolarization (0.1nA) activates a number of K^+ conductances (A, AHP) which leads to an outward rectification and causes a delay in action potential firing. *B*. Plot of averaged voltage responses to 900ms long current injections ranging from -0.1nA to 0.1nA for WT (black, n=52) and β_3 null (grey, n=47) relay cells at >P8. Both functions similar patterns of membrane rectification.

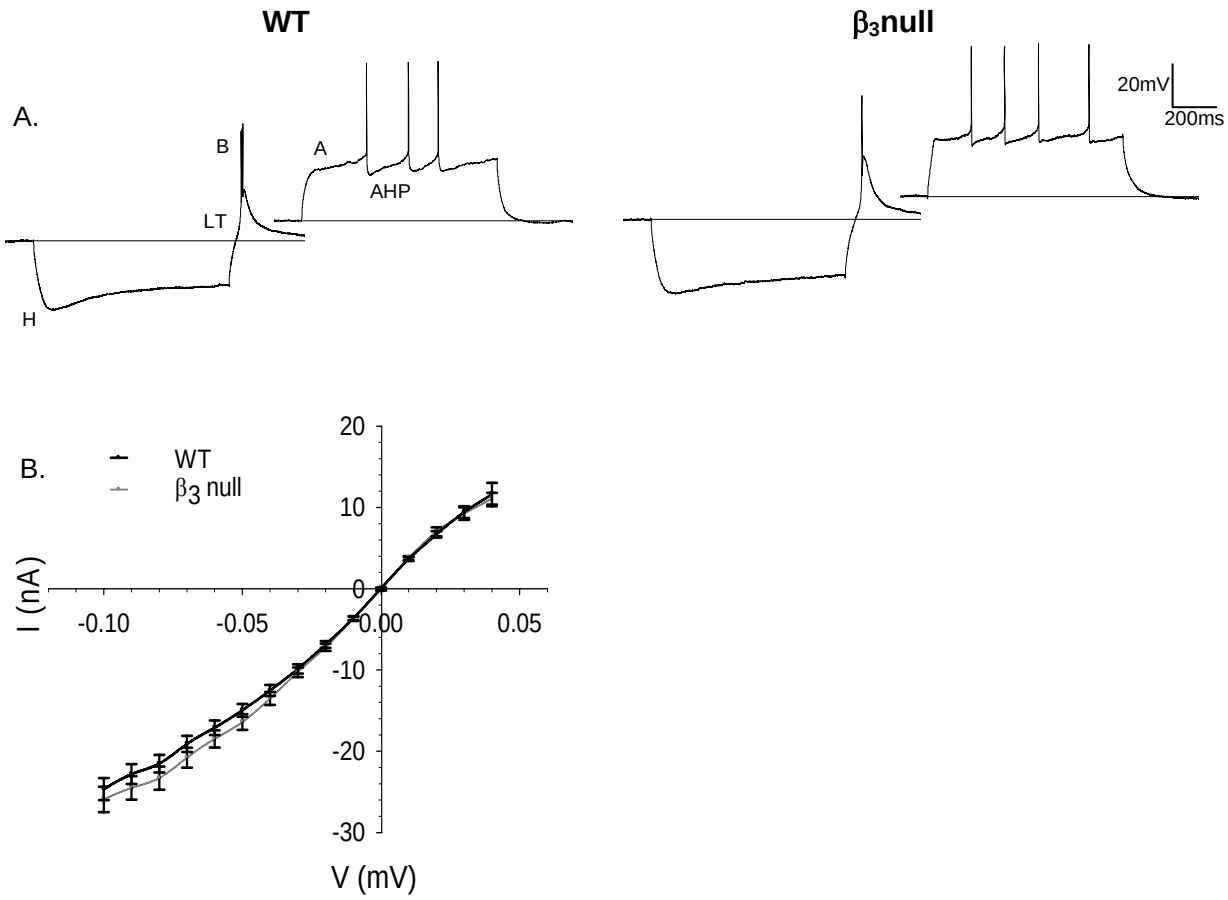

Discussion

We have shown that a number of converging events contribute to the developmental regulation of plateau potentials. These include the degree of retinal convergence, the pattern of retinal stimulation, the maturation of inhibition, and the density of functional L-type Ca^{2+} channels. Indeed, these elements undergo dramatic changes around the time of natural eye opening (Guido, 2008) thereby restricting the prevalence of plateau activity to the first two weeks of postnatal life. In the ensuing discussion we address each of these factors separately and then how the interplay between them regulates the generation of plateau potentials.

Excitatory synaptic connections undergo substantial pruning during the first few weeks of postnatal life such that the number of retinal inputs onto single dLGN cells is greatly reduced (Guido, 2008). At early ages (before P14), when the degree of retinal convergence is high, plateau potentials were readily evoked. Experiments in which the stimulus intensity and temporal frequency of OT stimulation were varied revealed that the summation of these convergent inputs was sufficient to activate plateau activity. In fact, at early ages, the summation of responses for cells with 5 or more inputs almost always led to plateau activity. Although each individual excitatory response is weak at this age (Chen & Regher, 2000), when summation occurs it leads to large, long lasting depolarizations (Lo *et al*., 2002; Jaubert-Miazza *et al*., 2005; Liu & Chen, 2008) that seem to favor the voltage- and time-dependent requirements for L-type Ca^{2+} channel activation (Kammermeier & Jones, 1997). Indeed, the underlying composition of these glutamatergic events are dominated by NMDA receptors that possess a subunit composition promoting a relaxed voltage dependency, slower decay kinetics, and increased synaptic charge transfer (Liu & Chen, 2008). In fact, the long decay times of NMDA receptor currents seem to augment summation, especially at low temporal rates, leading to high levels of depolarization

and plateau activation. By the second postnatal week, when dLGN cells receive far fewer retinal inputs, plateau activity was rarely observed. Despite the reduced convergence, individual retinal inputs are relatively strong and, in most cases, the peak amplitude of their synaptic current exceeds that of developing dLGN cells (Hooks & Chen, 2006). However, unlike the responses of early postnatal cells, those at older ages are dominated by fast, short-duration AMPA receptor activation that has reduced charge transfer (Liu & Chen, 2008).

The pruning of retinal inputs is also accompanied by the maturation of intrinsic inhibitory circuits. Both ultrastructrual and electrophysiological observations reveal that few, if any inhibitory synapses are present at young ages (Ziburkus *et al*., 2003; Bickford *et al*., 2010). However, by eye opening (P14), a feed-forward circuit involving retinal axons that innervate both intrinsic interneurons and relay cells is present. When this circuit is activated by OT stimulation, relay cells exhibit EPSPs that are followed by robust inhibitory responses (Crunelli *et al*., 1988; Lo *et al*., 2002; Ziburkus *et al*., 2003; Blitz & Regehr, 2005; Bickford *et al*., 2010). Our pharmacological experiments reveal that blocking the $GABA_A$ component of this inhibition increases the duration and amplitude of retinally evoked EPSPs. For cells recorded at older ages (after P14), this heightened depolarization can lead to a modest increase in the incidence of plateau activity, however, it still remains significantly lower than the incidence recorded at early ages. Thus, the emergence of inhibition per se cannot fully account for the age related decrease in plateau activity.

Finally, we examined the expression of the L-type Ca^{2+} channels as a contributing factor by utilizing a transgenic mouse in which the ancillary β_3 subunit of the L-type Ca^{2+} channel has been deleted. Previous studies indicate that β subunits play an important role in channel kinetics (Birnbaumer *et al*., 1998) and membrane insertion of L-type Ca^{2+} channels (Bichet *et al*., 2000),

and that the targeted deletion of the β_3 subunit results in a significant reduction in the L-type current. Estimates obtained in isolated dorsal root ganglion cell preparations reveal about a 60% reduction in the peak amplitude of the L-type Ca^{2+} current (Namkung *et al*., 1998). Although we did not measure L-type current directly in the dLGN of β_3 nulls, we found that protein expression levels of the pore forming alpha subunits to be reduced by 70% (α_{1C}) and 40% (α_{1D}) compared to age-matched WTs. Moreover, synaptically evoked plateau potentials were rarely observed in these mutants even at early ages or when repetitive stimulation was used. Thus, these experiments reveal that overall channel density and functional expression affect plateau activity. Interestingly, a similar scenario may occur during development. Both western blot analysis and immunostaining reveal that the density of L-type channels is highest at early ages, but then declines with age (see also Jaubert-Miazza *et al*., 2005).

While all of these events are contributing factors, it is difficult to assess how each, by itself, regulates the generation of plateau potentials. Nonetheless, it is our belief that no one single variable is solely responsible. Clearly, overall L-type Ca^{2+} channel expression is an overriding factor. However, we still are able to modulate the incidence of plateau activity during conditions of both high and low channel expression. For instance, during the peak of L-type expression (before P14), the incidence of plateau activity can be altered by summating post-synaptic events either in the spatial or temporal domain thus underscoring the importance of excitatory retinal convergence. Moreover, at a time when L-type expression is relatively low (after P14), the removal of inhibition leads to a substantial increase in incidence of plateau activity, suggesting that inhibition curtails the degree of depolarization needed to activate these events. Perhaps the latter is not surprising since even mature thalamic relay cells possess robust L-type Ca^{2+} currents (Hernandez-Cruz and Pape, 1989; Kammermeier and Jones, 1997; Zhou *et*

al., 1997; Budde *et al*., 1998). The relationship between overall channel expression and the maturation of retinogeniculate circuitry is further underscored when one considers the incidence of plateau potentials in β_3 nulls. First, plateaus in β_3 nulls are rare, but clearly more prevalent at young ages when factors such as retinal convergence and the lack of inhibition seem to have their greatest impact. Indeed, at late ages, when inhibition is peaking, far fewer plateau potentials are evoked in these mutants. Secondly, although L-type expression is lower in young postnatal β_3 nulls than in late postnatal WTs, the incidence of plateau potentials is actually higher in the mutants. This suggests that despite the low levels of channel expression, the functional state of early geniculate circuitry can still promote plateau activity.

In the adult dLGN, L-type activity has been reported to play a role in signal transmission by regulating cellular excitability during tonic firing modes (Zhou *et al*., 1997; Budde *et al*., 1998; Budde *et al*., 2002; Pape *et al*., 2004). However, the developmental regulation of plateau potentials suggests that L-type activity may also be associated with the activity dependent refinement of developing retinogeniculate connections. L-type Ca^{2+} channels are located primarily on the somata and proximal regions of dendrites (Zhou *et al*., 1997; Budde *et al*., 1998). Thus, their close proximity to retinal synapses (Rafols & Valverde, 1973; Sherman & Guillery, 2002; Bickford *et al*., 2010) allows for L-type activation to be coincident with retinally evoked postsynaptic events. In fact, the driving force behind their concerted activation could arise from spontaneous retinal waves. *In vitro* recordings of retinal waves in a preparation that preserves the eyes and retinal connections to dLGN reveal that groups of retinal ganglion cells firing in synchrony to generate long epochs of high frequency activity and large sustained depolarizations in dLGN cells (Mooney *et al*., 1996). Although the underlying pharmacology of these responses was not investigated, their profile largely resembles synaptically evoked plateau

activity generated by high frequency stimulation of OT (Lo *et al*., 2002; Butts *et al*., 2007). Thus it would seem that the high incidence of plateau activity coincides with a time during development when retinal waves prevail. In fact, plateau activity and its associated Ca^{2+} influx may represent the means by which retinal waves mediate the activity dependent refinement of retinogeniculate connections (Torborg & Feller, 2005).

In fact, the activity dependent influx of Ca^{2+} associated with L-type channel activation has been implicated in several forms of synaptic plasticity (Magee & Johnston, 1997; Lo & Mize, 2000; Guido *et al*., 2001) as well as signaling cascades involved in the structural remodeling of synaptic connections (Greer & Greenberg, 2008). Studies in developing dLGN show that L-type activation is needed for the induction of long-term changes in synaptic strength (Ziburkus *et al*., 2009) and seems to favor the Ca^{2+} dependent cAMP response element binding protein (CREB) signaling cascade (Mermelstein *et al*., 2000; Dolmetsch *et al*., 2001; Kornhauser *et al*., 2002) known to be important for retinogeniculate axon segregation (Pham *et al*., 2001). While a direct link between the activity-dependent refinement of retinogeniculate connections and L-type mediated plateau activity is presently lacking, the future utilization of the β_3 null mouse may offer an opportunity to directly assess this relationship.

Chapter 2

The absence of synaptically evoked plateau potentials in dorsal lateral geniculate nucleus relay cells leads to a breakdown in retinogeniculate refinement

Abstract

In developing dLGN relay cells, repetitive stimulation of the optic tract in a manner that mimics spontaneous retinal waves evokes long-lasting, high-amplitude depolarizations (plateau potentials), mediated by L-type calcium channels. Plateau potentials prevail early in life, at the peak of retinogeniculate refinement, and the large Ca^{2+} influx they generate could initiate remodeling. To determine whether synaptically evoked plateau potentials in dLGN are necessary for the refinement of retinogeniculate connections, we used a mouse that lacks the L-type Ca^{2+} channel β_3 subunit. These mutants have reduced L-type Ca^{2+} channel expression and current, and plateau potentials are rarely observed. *In vitro* multi-electrode array recordings of retinal explants reveal normal spontaneous waves. However, retinogeniculate projections in β_3 nulls fail to segregate properly and their dLGN cells show a higher degree of retinal convergence. Thus, postsynaptic L-type Ca^{2+} channel activity is necessary to implement the activity-dependent refinement of the retinogeniculate pathway.

Introduction

Over the past two decades much of our present understanding about the activity-dependent refinement of sensory circuits comes from studies that make use of retinogeniculate connections in the dorsal lateral geniculate nucleus (dLGN) of the thalamus. More recently, the retinogeniculate pathway of the mouse has emerged as a powerful model system, where the projections from the two eyes in dLGN are initially diffuse and overlapping, but become organized into non-overlapping domains just before eye opening (postnatal day (P) 12; Guido, 2008). Eye-specific segregation is accompanied by a pruning of retinal inputs onto single dLGN cells from as many as a dozen or so weak ones to 1-3 strong connections (Chen & Regehr, 2000; Jaubert-Miazza *et al*., 2005). Such remodeling has been attributed to spontaneous bursts of action potentials among neighboring retinal ganglion cells (RGCs) that spread as a wave across the retina (Torborg & Feller, 2005). Retinal waves are capable of driving robust post-synaptic excitatory activity in dLGN relay cells (Mooney *et al*., 1996) until about the time of natural eye opening, when visual evoked events serve as the primary source of dLGN activity (Demas *et al*., 2003).

When retinal waves are disrupted or eliminated, retinogeniculate projections fail to develop properly (Torborg & Feller, 2005; Huberman *et al*., 2008). For example, mice lacking the β2 subunit of neuronal nicotinic acetylcholine receptors do not exhibit normal stage II cholinergic retinal waves (~P1-10; Bansal *et al*., 2000). As a result, retinal projections from the two eyes initially remain diffuse and fail to segregate into eye-specific domains (Muir-Robinson *et al*., 2002). Another transgenic model, the no-b wave mouse (nob), has normal stage II waves but abnormal glutamatergic phase III waves that persist past the period of natural eye opening (Demas *et al*., 2006). While their projections in dLGN initially segregate, the prolonged, high

frequency waves cause the newly established eye-specific domains to return to a diffuse state. Together these studies suggest that there are two periods of activity-dependent refinement in dLGN, an initial, inductive phase during which eye-specific domains are formed and retinal pruning begins, and a maintenance phase, during which continued retinal activity is necessary for the connections to prune weak synapses and strengthen others (Guido, 2008; Huberman *et al*., 2008).

Despite the evidence linking retinal waves to retinogeniculate refinement, it is still unknown how such remodeling is implemented on a cellular level. A likely candidate involves the cAMP response element (CRE) binding protein (CREB), a transcription factor regulated by Ca^{2+} and cAMP. CREB-mediated gene expression peaks during dLGN refinement, and is important for retinogeniculate segregation (Pham *et al*., 2001). While NMDA receptors (NMDAR) could provide an activity-dependent Ca^{2+} influx to initiate CREB signaling cascades and have been shown to figure prominently in the developmental plasticity of many other sensory systems, they are not necessary for post-synaptic activity in developing dLGN cells (Mooney *et al*., 1996) nor the eye-specific segregation of retinal projections (Smetters *et al*., 1994). A more likely candidate is the high threshold L-type Ca^{2+} channel. Interestingly, its carboxyl tail directly binds calmodulin (CaM), a calcium binding protein that can activate CaM-dependent kinases to phosphorylate CREB, initiating gene transcription (Morad & Soldatov, 2005). This could initiate the pruning and stabilization of developing retinogeniculate connections in an activity- and Ca^{2+}-dependent manner.

In the dLGN, L-type Ca^{2+} channels are located primarily on the soma and proximal dendrites of relay cells (Budde *et al*., 1998; Jaubert-Miazza *et al*., 2005), thus placing them in close proximity to retinal synapses (Rafols & Valverde, 1973). Repetitive stimulation of optic

tract (OT) fibers in a manner that approximates retinal waves evokes a long lasting depolarization of sufficient amplitude and duration to activate high-threshold L-type Ca^{2+} channels (Lo *et al*., 2002). These events, called plateau potentials, occur more readily at young ages during the peak of retinogeniculate remodeling (before P14). A number of factors seem to contribute to the prevalence of this activity at early ages (Dilger *et al*., submitted), including the density of L-type expression (Jaubert-Miazza *et al*., 2005), the emergence of intrinsic feed-forward inhibitory activity (Bickford *et al*., 2010), the degree of retinal convergence (Chen & Regehr, 2000; Lo *et al*., 2002; Jaubert-Miazza *et al*., 2005; Hooks & Chen, 2006) as well as the changes in the subunit composition of excitatory receptors (Lui & Chen, 2008). Thus, the strong postsynaptic depolarization of dLGN cells provided by retinal waves coupled with the coincident activation of L-type Ca^{2+} channel plateau potentials seems a likely candidate for mediating activity-dependent remodeling in dLGN.

To test if the L-type mediated plateau potentials and their associated Ca^{2+} influx play a role in retinogeniculate refinement, we took a loss of function approach and made use of a mutant mouse that lacks the β_3 subunit of the L-type Ca^{2+} channel (Namkung *et al*., 1998). This accessory subunit is important for channel trafficking, and without it, there is a significant reduction in the membrane expression of the pore forming, α_{1C} subunit (Bichet *et al*., 2000), and, as a consequence, a greatly reduced L-type current (Namkung *et al*., 1998; Shiraiwa *et al*., 2007). Although these mutants show a decreased incidence in plateau potential activity, dLGN cells have normal intrinsic membrane properties and synaptic responses, comprised of EPSPs followed by IPSPs (Dilger *et al*., submitted). In fact, by all accounts, many aspects of their central nervous system (CNS) are indistinguishable from wild-type mice (WT; Namkung *et al*., 1998; Murakami *et al*., 2002; Shiraiwa *et al*., 2007; Dilger *et al*., submitted). For example, the

lack of the β_3 subunit does not seem to affect the retina, where the β_2 subunit is dominant (Ball *et al*., 2002). The structure and functional composition of the retina is also normal in β_3 nulls, as is their light response, which displays a normal electroretinogram b-wave. Thus, the β_3 null seems like a strong candidate to assess whether L-type Ca^{2+} channel activity is necessary for the refinement of dLGN connections.

In order to examine synaptically evoked L-type activity in β_3 nulls, we performed whole-cell current clamp recordings in a thalamic slice preparation that preserves the OT and its connections to the dLGN. As shown previously (Dilger *et al*., submitted), electrical stimulation of the OT failed to evoke synaptic plateau potentials in the majority dLGN cells of β_3 nulls, even at early postnatal ages. We also verified that spontaneous retinal activity in the β_3 null is indistinguishable from normal WTs by performing multi-electrode array recordings on retinal whole-mount explants. Finally, we assayed two aspects of refinement, eye-specific segregation and retinal convergence. To visualize eye-specific domains in dLGN, we made use of anterograde tracers in the form of cholera toxin subunit B (CTB) conjugated to different fluorescent markers, injected into one eye or the other. To determine the degree of retinal convergence, we obtained estimates of the number of retinal inputs converging onto single dLGN using the thalamic slice preparation. β_3 nulls show significantly less eye-specific segregation in dLGN and individual relay cells receive far more retinal inputs than age-matched WTs, indicating that the activity of the L-type Ca^{2+} channel plays a major role in mediating the activity-dependent refinement in dLGN.

Methods

All procedures were performed in compliance with the Institutional Animal Care and Use Committee at Virginia Commonwealth University. Wild-type C57/BL6 mice and a transgenic strain bred on a C57/BL6 background that lacks the β_3 subunit of the L-type Ca^{2+} channel (Namkung *et al*., 1998) were used. The mice were bred and housed in resident colonies and ranged in age from P7 to P34.

For methods on slice preparation, in vitro electrophysiology and estimates of retinal convergence see pages 12-14.

Multielectrode array recordings were carried out as reported previously (Demas *et al*., 2003; Demas *et al*., 2006). We prepared retinas in a room with only infrared illumination. After 1 hour of dark adaptation, mice were deeply anesthetized with isoflurane and decapitated, and the retina was removed in cooled, oxygenated ACSF (in mM: NaCl 119, KCl 2.5, $MgCl_2$ 1.3, $CaCl_2$ 2.5, NaH_2PO_4 1.0, glucose 11, and HEPES 20. A piece of retina was placed, ganglion cell side down, onto a 60-channel MEA (MultiChannel Systems), held in place with a lightly weighted insert filter (Corning), and superfused with oxygenated ACSF (1-2ml/min), maintained at 31-33°C. The ITO array electrodes were 30μm in diameter, arranged on an 8x8 rectangular grid with 100μm interelectrode spacing and 10μm electrode area. The retina was allowed to settle for 1 hour before recordings, which were done in complete darkness. Analog data was acquired at 25 kHz per channel. Antagonists DNQX (AMPAR, Tocris 2312), D-APV (NMDAR, Tocris 0106) and DHβE (neuronal α_4 subunit containing nicotinic receptor, Tocris 2349) were bath applied at 25μM. A threshold of six times the standard deviation of the noise was set for each channel, and 1ms of data before a threshold-crossing event and 3ms after the threshold event was stored for each waveform. These spike waveforms were then sorted with MCRack window method. The

burst and correlation analysis was preformed with Neuroexplorer, Excel, and custom Matlab software, as previously published (Demas *et al*., 2003; Demas *et al*., 2006).

Intravitreal eye injections. Mice are anesthetized by hypothermia (<P4), with isoflurane vapors (P4-P27) or injected IP with Ketamine/ Xylazine (>P27). Using a dissecting microscope, the sclera and cornea are pierced with a glass pipette and excess vitreous is drained. Another pipette, filled with a 1% solution of a fluorescent conjugate (Alexa Fluor 488 or 555) of CTB (Invitrogen) in distilled water is inserted into the hole made by the initial pipette. The pipette is attached to a picospritzer and a prescribed volume (1-4µl at P1-P10 and 5-8µl at >P10) of solution is injected into the eye. Mice are given a 2-3 day survival period sufficient for the tracer to reach and fill the dLGN and superior colliculus. Animals are then deeply anesthetized with isoflurane and transcardially perfused with phosphate buffer saline for 5 minutes and 4% paraformaldehyde in 0.1M phosphate buffer for 25 minutes. Brains are removed, post-fixed overnight and sectioned (70µm) in the coronal plane using a vibratome (Leica VT1000S). Sections containing the dLGN are mounted with ProLong Gold Antifade Reagent (Invitrogen) and visualized with fluorescent microscopy. Images of dLGN are acquired with a Photometrix Coolsnap camera attached to a Nikon Eclipse fluorescence microscope using a 10x objective. Fluorescent images of labeled sections are acquired and digitized separately (1300 x 1030 pixels /frame) using the following filter settings: Alexa 488: Exciter 465-495, DM 505, BA 515-555, Alexa 594: Exciter 528-553, DM 565, BA 600-660. To measure the spatial extent and the degree of overlap of crossed and uncrossed projections, threshold-imaging protocols are used (Jaubert-Miazza *et al*., 2005). An R-analysis, based on the log ratio of pixel intensity is used to assess the degree of segregation between crossed and uncrossed projections (Demas *et al*., 2006).

Results

Prevalence and kinetics of plateau potentials in WTs and β_3 nulls

In adult dLGN cells of WTs, synaptic responses to a single, near threshold electrical pulse delivered to the OT typically evokes an EPSP followed by IPSP activity (Fig. 2.1A, *left*). However at young ages, when suprathreshold stimulation is applied, plateau potentials can be evoked (Dilger *et al*., submitted). This long lasting, high amplitude depolarization is mediated by the L-type Ca^{2+} channel, and is a salient characteristic of developing dLGN cells, occurring almost exclusively before eye-opening (P14). Plateau activity can also be evoked using repetitive stimulation. Using stimulus intensities that generate an EPSP of approximately half maximum amplitude, and repetitive stimulation at 20, 50 and 100Hz, these responses occur frequently at young ages (Fig. 2.1B, *left*). While dLGN cells of β_3 nulls exhibit the normal complement of EPSP/IPSP activity, plateau potentials are rarely evoked (Fig. 2.1A, *right*; Dilger *et al*., submitted). Figure 2.1C plots the incidence of plateau activity in WTs and β_3 nulls before P14. In WTs, a plateau potential was evoked in 18 out of 38 cells (47%) with a single stimulation and in 61% to 67% of cells with 20-100Hz repetitive stimulation. In contrast, in β_3 nulls, plateau potentials were never evoked with a single stimulus, were rarely seen with 20 and 50Hz (4-8% of cells) and even the highest rate of 100Hz stimulation evoked far fewer plateau potentials compared to WTs (38%).

The plateau potentials that were evoked in β_3 nulls seemed to have different kinetics than those in WTs (Fig. 2.2A) suggesting that the overall influx of Ca^{2+} is different in these mutants (Birnbaumer *et al*., 1998; Dolphin, 2003). We measured plateau activity evoked in a total of 24 cells (15 WT and 9 β_3 null) using 100Hz rate of stimulation. For this analysis we measured amplitude, rise, decay and duration (see inset Fig. 2.2A). Amplitude was measured at the trough

of inactivating Na^+ spikes during the peak of the plateau activity, and was reduced by almost 10mV in β_3 nulls (Fig. 2.2B, WT: 51.9mV; β_3 null: 42.2mV; Student's t-test $p<0.001$). Rise time, measured as the first 50ms of the response, was also compared (Fig. 2.2C, *left*). Each response was fit to a linear best-fit line, and the slopes of these were averaged (Fig. 2.2D, *left*). Plateaus in WTs had significantly faster rise times than those in β_3 nulls (WT: 1.3mV/ms; β_3 null: 0.65mV/ms; Student's t-test $p<0.001$). To analyze the decay times, the first 50ms after the inactivating Na^+ spikes was fit with a single exponential decay curve (Fig. 2.2C, *right*). The decays of β_3 null plateaus were significantly slower than those in WTs (Fig. 2.2D, *right*; WT τ: 19.5ms; β_3 null τ: 24.9ms; Student's t-test $p<0.001$). We measured duration in two ways. First, we examined the duration form onset to 10% of maximal amplitude. Since the decay of plateau potentials in β_3 nulls was slower, an increase in this measure of duration was expected (not shown; WT: 237ms; β_3 null: 423ms; Student's t-test $p<0.001$). However, since L-type Ca^{2+} channels are only activated at depolarized membrane potentials, we also looked at the duration of the plateau potential from onset to just prior to the start of decay (i.e. the end of the inactivating Na^+ spikes). Interestingly, there were no differences in this measure of duration (not shown; WT: 115ms; β_3 null: 128ms; Student's t-test $p>0.1$), suggesting that the activation times of L-type Ca^{2+} channels were not prolonged in β_3 nulls.

Developmental composition of NMDAR and AMPAR synaptic currents

Excitatory synaptic currents at the retinogeniculate synapse undergo a number of changes during early postnatal life including in their relative strength and receptor subunit composition (Liu & Chen, 2008). It is conceivable that the alterations in the incidence and kinetics of plateau potentials in β_3 nulls could be related to defects in these events. To determine if the loss of the β_3 subunit had any effect on these properties, we performed voltage-clamp recordings at –70mV, to

examine the fast inward AMPA receptor current, and at +40mV, to see the slowly decaying outward NMDA receptor current (AMPAR and NMDAR, respectively). Studies in the dLGN have shown changes in the ratio of the currents with age, with the NMDAR current decreasing relative to the AMPAR current (Liu & Chen, 2008). Figure 2.3A compares representative maximal AMPAR to NMDAR current ratios recorded at different postnatal ages for WT and β_3 null dLGN cells, normalized to NMDAR currents. In both WTs and β_3 nulls, NMDAR currents dominate at P9-11 (Fig. 2.3B; β_3 null (WT): 0.96 (0.98) one-way ANOVA: $p>0.1$), with AMPAR currents strengthening with age (P15-17 β_3 null (WT): 1.76 (1.65) $p>0.1$; P9-11 vs. P15-17 for both WT and β_3 null one-way ANOVA: $p<0.001$). Thus, developmental changes occur normally in β_3 nulls. Additionally, the maximal current evoked from AMPAR and NMDAR was not different between WT and β_3 null (not shown; β_3 null (WT): AMPA P9-11: –0.75±0.03nA (–0.84±0.07nA); P15-17: –1.0±0.1nA (–1.0±0.1nA); NMDA P9-11: 0.82±0.04nA (0.88±0.06nA); P15-17: 0.63±0.08nA (0.63±0.07nA); one-way ANOVA $p>0.1$ for all WT vs. β_3 null comparisons).

Previous studies at the retinogeniculate synapse also show that the decay time of NMDAR accelerates with age (Lui & Chen, 2008), caused by changes in NR2 subunit composition from the slowly decaying NR2B to the faster NR2A. Figure 2.3C shows representative maximal NMDAR currents at early (P10) and late (P16) postnatal ages in the WT and β_3 null. In both strains, relay cells at young ages decayed more slowly (WT: 144ms; β_3 null: 145ms; one-way ANOVA: $p>0.1$) than those at older ages (WT: 96.7ms; β_3 null: 87.4ms; one-way ANOVA: $p>0.1$; both strains P9-11 verses P15-17: $p<0.001$). These results, as well as the relative strengthening of AMPAR currents with age, indicate that glutamatergic transmission at the retinogeniculate system of β_3 nulls develops normally. Moreover, the decreased incidence

and kinetics in plateau potentials noted previously are not due to a lack of excitatory drive but instead reflect defects in either the channel assembly or membrane insertion.

Spontaneous retinal activity in β_3 nulls

While visual responses in β_3 nulls do not seem to be impaired (Ball *et al*., 2002), the patterns of spontaneous retinal activity prior to eye opening remain unexplored. To address this, we performed *in vitro* multi-electrode array recordings of retinal explants from β_3 nulls. The firing rate and interwave intervals seen in P7 and P12 β_3 nulls are comparable to those previously recorded in WTs (*cf.* Demas *et al*., 2003; Demas *et al*., 2006; P7 (P12) firing rate: 0.57±0.07Hz (0.48±0.07Hz); interwave interval: 73.4±5.7s (20.6±1.4s)). At P7, RGCs fire in bursts, which are separated from each other by about a minute (Fig. 2.4A). At this age, waves are cholinergic in nature, and, as expected, bath application of two glutamatergic antagonists, DNQX, which blocks AMPAR, and D-APV, an NMDAR blocker, had no effect on the waves, while DHβE, a cholinergic antagonist, eliminated them (Fig. 2.4B). By P12, the interwave interval had decreased to less than half a minute (Fig. 2.4A), and pharmacology revealed the reported developmental switch from cholinergic to glutamatergic driven activity (Fig. 2.4B). At this age, DHβE had no effect on the wave activity, while application of D-APV and DNQX eliminated the waves. Spatial temporal correlations of activity among neighboring RGCs was also assessed in β_3 nulls. The degree to which developing RGCs fire together typically depends upon the distance separating the two cells (Demas *et al*., 2003). This was assessed for pains of cells as a function of the estimated distance between them, which was obtained by the position of the electrode from which the cell was recorded. At both P7 and P12 the correlation index between neighboring RGCs firing time decreased as a function of inter-cell distances (Fig. 2.4C). Additionally, we calculated the coherence of cell pairs to assess how correlated their activity is at a particular

frequency. At P12, the mean coherence was 0.15Hz, corresponding to the frequency of bursting typically seen at this age in WTs (see Demas *et al*., 2003).

Retinogeniculate refinement in WTs and β_3 nulls

To determine whether the lack of plateau potentials in β_3 nulls affect eye-specific segregation in the dLGN, we made intraocular eye injections of CTB conjugated to two different fluorophores (Alexa Fluor 594 or 488). This technique allows for the simultaneous visualization of terminal domains occupied by contralateral and ipsilateral projections as well as the overlap between them (Torborg & Feller, 2004; Jaubert-Miazza *et al*., 2005). Examples of the labeling pattern in WT and β_3 nulls at different ages are shown in Figure 2.5A (contralateral: red; ipsilateral: green; overlap: yellow). In WTs, by P11 the regions of dLGN occupied by contralateral and ipsilateral projections are well defined and showed little overlap (4±0.3%). Ipsilateral projections only make up a small portion (11±0.5%) of the territory, and are confined to a small patch in the dorsal-medial region of the dLGN. However, in β_3 nulls, the ipsilateral eye projections were more diffuse, even as late as P28 (7±0.4%). Additionally, ipsilateral domains were greatly expanded (17±0.8% at P28) particularly along the ventral-medial aspect of dLGN. By binarizing images of the dLGN (Fig. 2.5A, *center columns*), we were able to quantify the spatial extent of the ipsilateral patch as well as the amount of overlap between the projections (Fig. 2.5C). We found that the ipsilateral projection as well as the degree of overlap was significantly larger in β_3 nulls than in age-matched WTs. This defect was seen across all ages studied, including as late as P28. For example, in Figure 2.4D the overall average of the ipsilateral eye projection and the degree of overlap was significantly larger in β_3 nulls than WTs (β_3 null (WT): ipsilateral: 16±0.4% (12±0.4%); overlap: 7±0.2% (4±0.3%); Student's t-test both ipsilateral and overlap, $p<0.001$)

Eye-specific segregation can also be quantified by analyzing the fluorescent intensity of individual pixels (Torbor & Feller, 2004; Jaubert-Miazza *et al*., 2005; Demas *et al*., 2006). For each pixel in a labeled section of dLGN (Fig. 2.5A, *edges*), we calculated the logarithm of the ratio of fluorescent intensities for ipsilateral (F_I) and contralateral (F_C), called the R-value ($R=\log[F_I/F_C]$). Averaged histograms of the R-values for labeled sections of WTs and β_3 nulls at P17 and P28 are shown in Figure 2.5E. The WT distributions are typically wide and have two peaks, one around –1 representing pixels from contralateral terminal fields with and a smaller peak around +1 representing the pixels from ipsilateral eye fields. These distributions also have a trough around 0, the value that represents pixels with high intensities for both the contralateral and ipsilateral fluorescence (Torborg & Feller, 2004). Distributions from WTs have typically large variances, or ranges of R-values, indicating more contralateral-dominant and ipsilateral-dominant pixels, and therefore more segregation. Variance is plotted as a function of age in Figure 2.5F. As early as P11, WTs have high variances in their R-distributions, indicating that their projections are well segregated. β_3 nulls, however, have much narrower R-distributions with significantly smaller variances, indicating that they have more pixels containing both contralateral and ipsilateral domains, and thus far less segregation. The average R-distribution in β_3 nulls only has one peak (around –0.5) even as late as P28 (Fig. 2.5E), and their variances are significantly lower across all ages (Fig. 2.5G; β_3 null (WT): 0.4±0.01 (0.5±0.01); Student's t-test, $p<0.001$).

We also wanted to examine whether these diffuse projections have a functional consequence, that is, if individual relay cells in β_3 nulls have a higher degree of retinal convergence. Moreover, we wanted to assess whether coarse (anatomical segregation) as well as fine scale (pruning of individual retinal inputs) refinement is affected in β_3 nulls. To accomplish this, we examined the

synaptic responses of WT and β_3 nulls at different stimulus intensities. Such protocols are used to obtain estimates of retinal convergence on individual relay cells (Jaubert-Miazza *et al*., 2005; Hooks and Chen, 2006). Figure 2.6 shows the EPSP or EPSC amplitude by stimulus intensity plots of four WT and four β_3 null cells. Accompanying each plot are the corresponding synaptic responses (*inset*). In WTs at young ages (P7, top left), the stimulus intensity plots are graded, indicating a high degree of retinal convergence (Jaubert-Miazza *et al*., 2005). With age, inputs are pruned and by P16 or so, this graded profile changes and becomes more step-like. However, in the β_3 null mouse, the profiles remain graded, indicating a high degree of retinal convergence even at late postnatal ages. These relations are summarized in Figure 2.7, which plots estimates of retinal convergence for all cells recorded in WTs and β_3 nulls. In WTs, there is an age related decrease in retinal convergence such that at early ages (P7) cells have 6-10 inputs and later (P18 and above) only 1-3. By contrast, in β_3 nulls cells have more inputs at early ages and undergo far less pruning such that even at P31 as many as 10 can be seen (single exponential fits: Two-Sample Kolmogorov-Smirnov Test $p<0.001$). These relationships are summarized more quantitatively in Figure 2.7B. On average, when cells are grouped by postnatal day, β_3 nulls have more inputs at P7-9 (β_3 null [WT]: 14±0.3 [8±0.6]), P10-12 (7±0.4 [5±0.4]) and P16+ (4±0.4 [2±0.2]) (one-way ANOVA $p<0.01$).

Figure 2.1

Synaptic responses of developing dLGN cells: WTs and β_3 nulls.

A. Synaptic responses of dLGN cells evoked by a single electrical pulse delivered to the optic tract (OT) in WTs (*left*) and β_3 nulls (*right*). (*Top*) At P18, near threshold stimulation activates an EPSP followed by IPSP activity in WTs and β_3 nulls. (*Bottom*) At P11, maximal levels of stimulation triggers plateau activity in WTs, but not in β_3 nulls. *B.* Synaptic responses using repetitive stimulation (5 pulses of 20, 50 and 100Hz). In WTs, plateau activity is readily evoked at P14 (*left*). By contrast in β_3 nulls, plateau activity is rarely seen even at young ages such as P10, and only with high repetitive stimulation (100Hz). Responses in *A*-*B* recorded at –60mV. *C.* Summary plot showing the incidence of plateau potentials encountered before P14 in WTs (black) and β_3 nulls (red). This incidence of plateau potentials is greatly reduced in β_3 nulls.

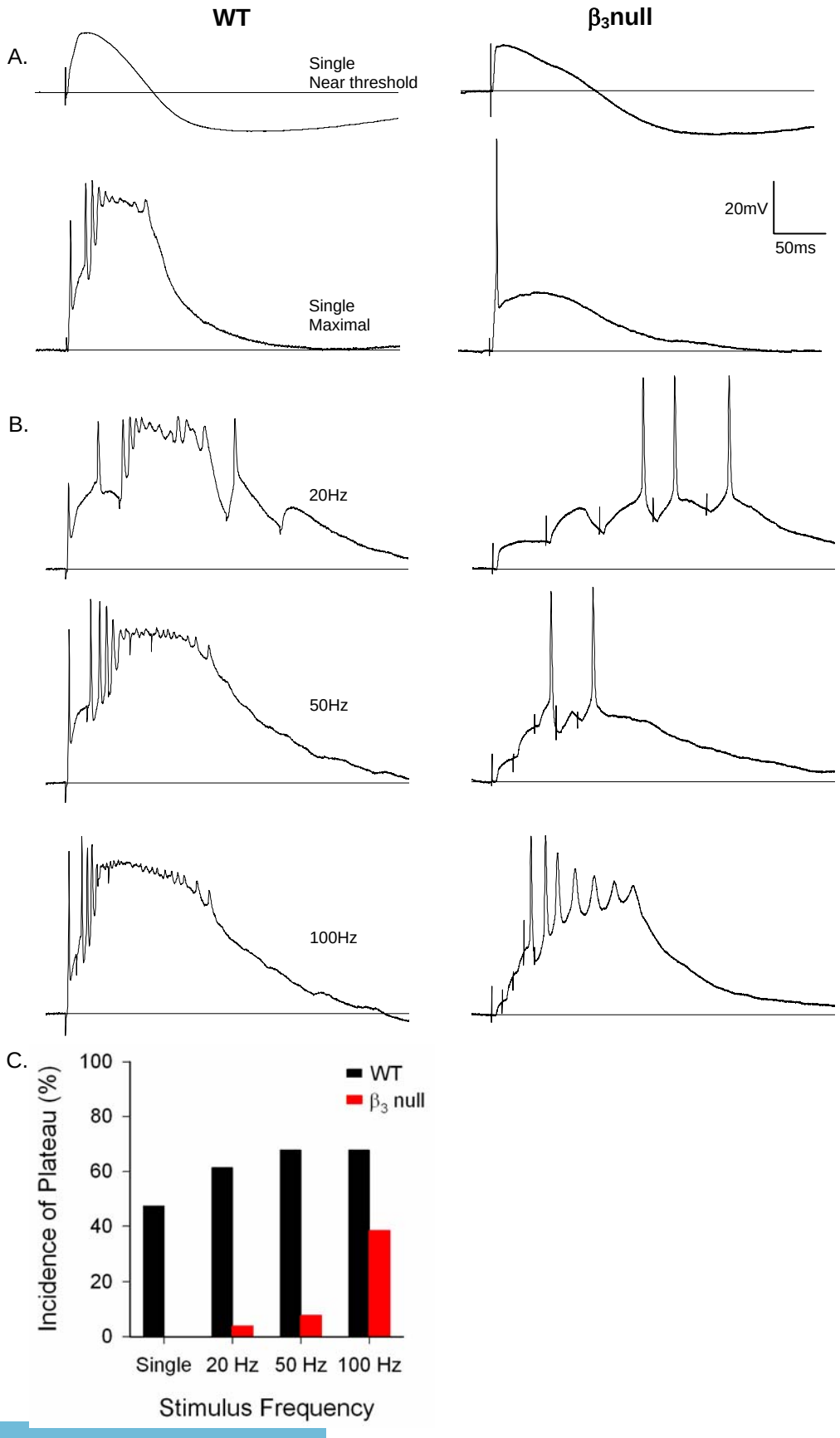

Figure 2.2

Amplitude and kinetics of plateau potentials in WTs and β_3 nulls.

A. Representative plateau potentials stimulated with 5 pulses at 100Hz at –60mV in WTs (*top*) and β_3 nulls (*bottom*). Although stimulation is able to evoke plateau activity in β_3 nulls, they have different kinetics than plateaus recorded in WT do. Inset, schematic depicting the following measurements: amplitude (1), rise (2), decay (3), duration to 10% (4) and duration to decay onset (5). *B.* Mean and S.E.M. of the amplitude (mV) of plateaus in WTs and β_3 nulls, measured at the peak amplitude of the plateau potential (i.e. at the troughs of the inactivating Na^+ spikes). Plateaus in β_3 nulls are smaller in amplitude compared to WTs. *C.* Plots of the rise (*left*) and decay (*right*) of plateau activity in WTs (*top*) and β_3 nulls (*bottom*). Rise plots depict the first 50ms of response, decay the first 50ms after the last inactivating Na^+ spike. Thin grey lines show raw traces, thick black and red lines depict averaged response. Plateaus in the β_3 nulls rise and decay more slowly compared to WTs. *D.* Mean and S.E.M. of the rise slope (mV/ms, *left*) and the decay τ (ms, *right*, fit to a single exponential) in WT (black) and β_3 nulls (red). Plateaus in the β_3 nulls have a slower rise and decay. β_3 null and (WT) cells: 9 (15).

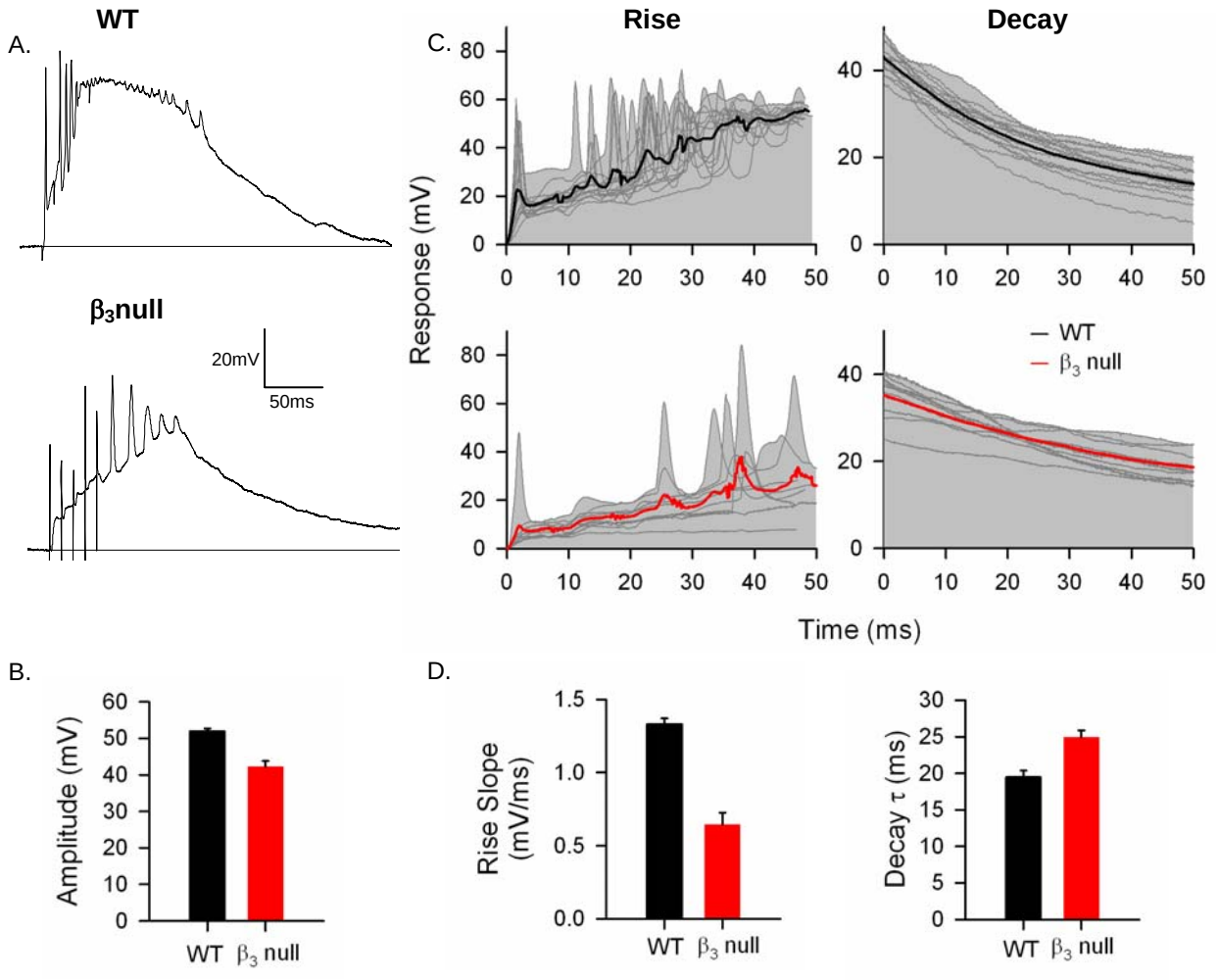

Figure 2.3

AMPA and NMDA responses in developing dLGN cells in WTs and β_3 nulls.

A-B. Representative maximal current traces at –70 (inward) and +40mV (outward) at P10 and P15 in WT (black) and β_3 nulls (red; *A*). Mean and S.E.M. AMPAR/NMDAR current ratio in mice from P9-11 and P15-17 in WT and β_3 nulls (*B*). In both WTs and β_3 nulls AMPAR/NMDAR current ratios increase with age. *C-D*. Representative NMDAR current traces in P10 and P16 WTs and β_3 nulls (*C*). Mean and S.E.M. decay τ values (ms, determined with a single exponential fit), showing NMDAR currents decay faster at older ages in both WTs and β_3 nulls (*D*). Traces in *A* and *C* are recorded in the presence of bicuculline, CGP and nimodipine and normalized to peak NMDA current. β_3 null and (WT) cells: P9-11 ratio: 26 (21); τ: 37 (29); P15-17 ratio: 22 (19); τ: 35 (29).

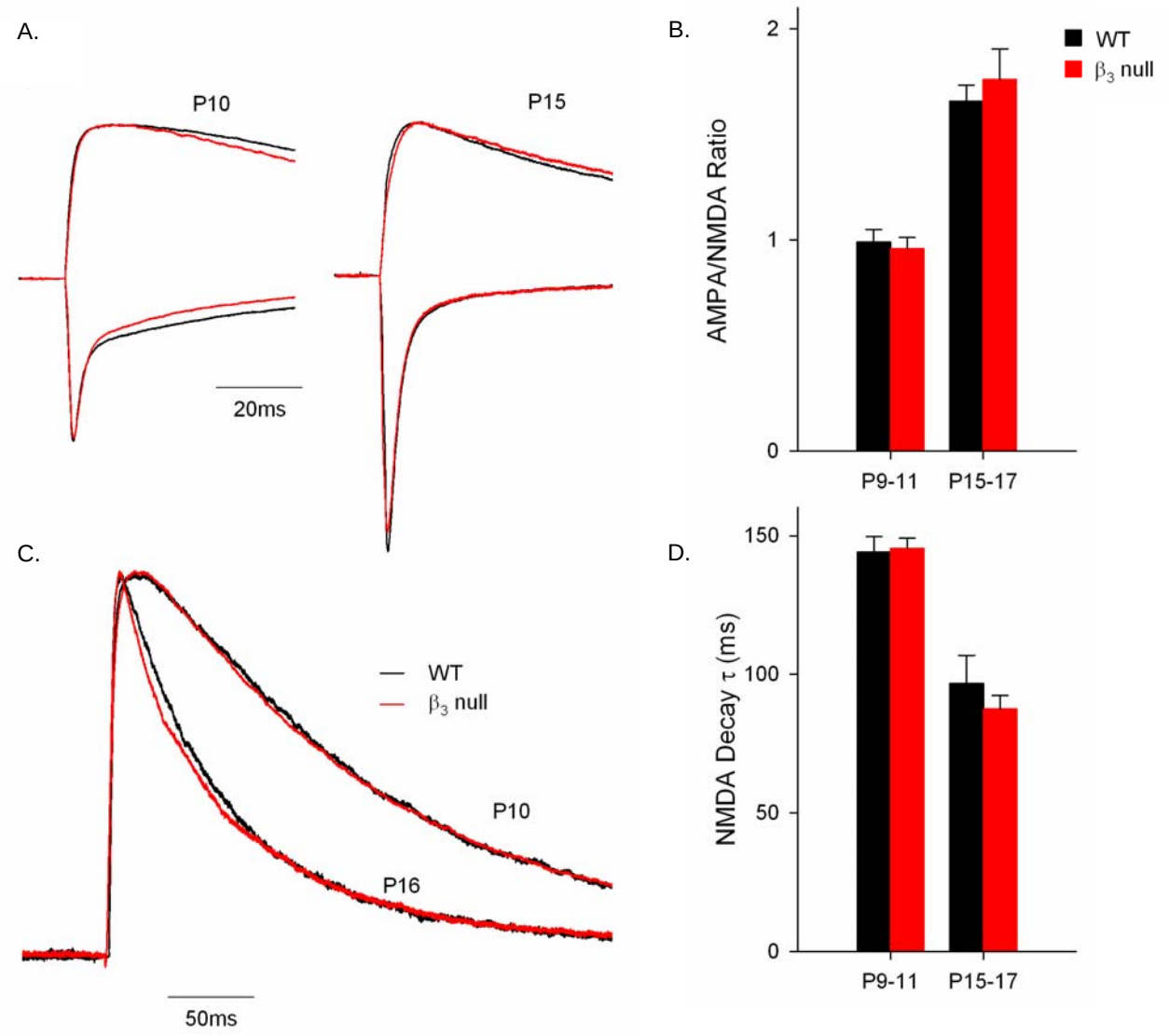

Figure 2.4

Retinal waves in β_3 nulls.

A. Rasters depicting spike trains for 30 simultaneously recorded RGCs from β_3 null retinas at P7 and P12. Below, a histogram of the population firing rate of all cells, binned per second. At both ages, the patterning of waves is indistinguishable from WT (*cf.* Demas et al, 2003; 2006). *B.* Representative response histograms demonstrating underlying pharmacology of retinal waves. At P7, waves continue in the presence of the glutamertic antagonists DNQX and D-APV, but are blocked by the cholinergic antagonist DHβE. At P12, waves continue in the presence of DHβE but are blocked by DNQX and D-APV, revealing their glutamertic drive. *C.* Plots showing correlation indices (logarithmic scale) between pairs of cells (2,300 from 3 mice at P7; 1,600 from 3 mice at P12), with each dot representing one pair, as a function of the estimated distance separating the pair. The linear best-fit line indicates that the further a pair of cells are from each other, the less likely they are to fire together.

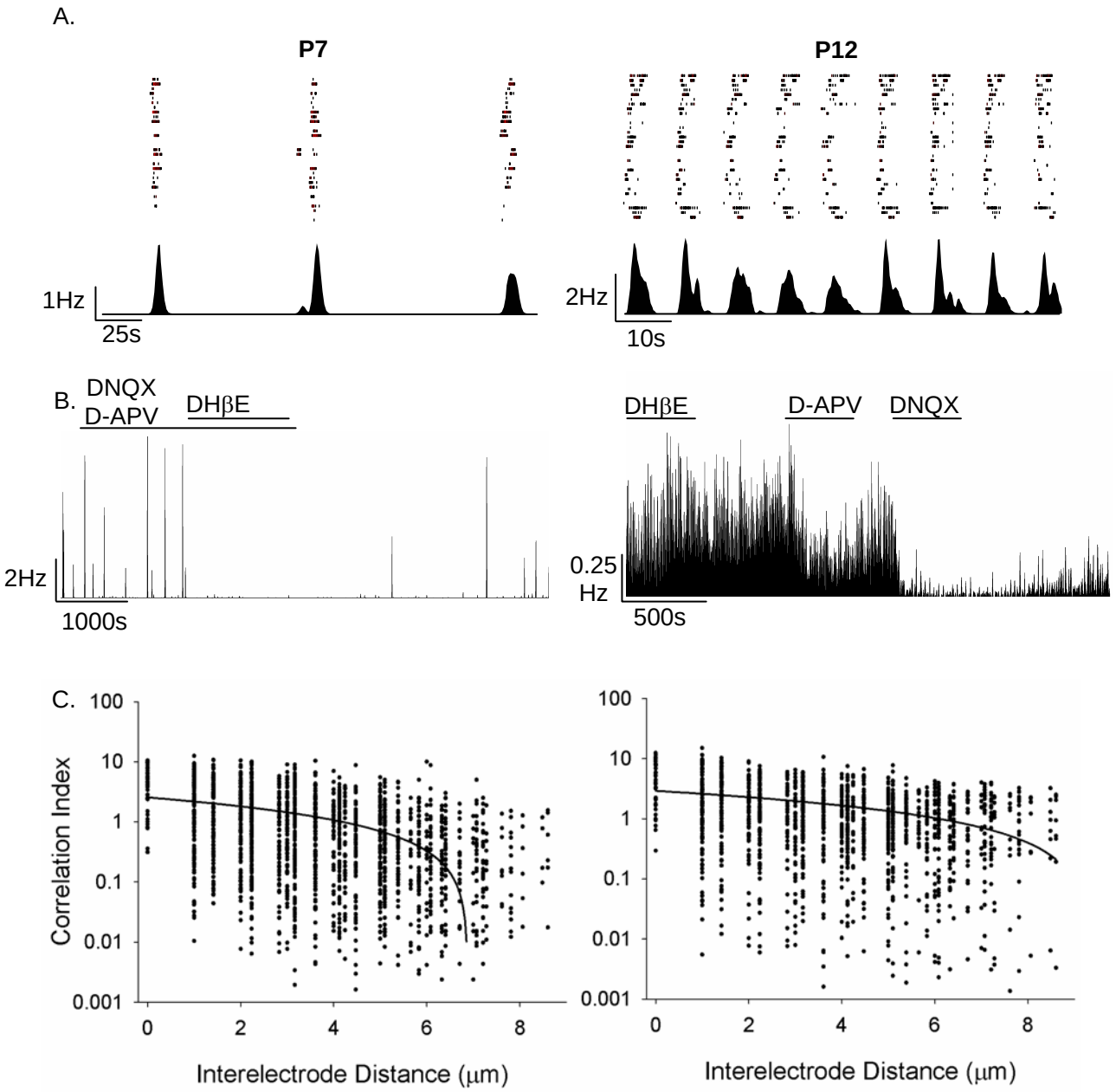

Figure 2.5

Eye-specific patterning in WTs and β_3 nulls.

A. Representative coronal sections from the dLGN of WTs and β_3 nulls at P11, P17 and P28. Shown are the retinal terminal fields for contralateral (red) and ipsilateral (green) eyes. Binarized representations of each dLGN (central columns) more clearly demonstrate the innervation patterns of each eye, as well as the regions where they overlap (yellow). At P11, WTs display eye-specific segregation with little overlap; however terminal fields in β_3 nulls continue to be diffuse and overlapping as late as P28. *B.* Ipsilateral projections from three consecutive sections in a P21 and a P28 β_3 null, from rostral to caudal. Ipsilateral projections in β_3 nulls maintain expanded ipsilateral eye projections throughout the dLGN. Sale bar for images in *A-B*: 100μm. *C.* Plots of the percent area of dLGN occupied by the ipsilateral eye (*left*) and the overlap between the projections from the two eyes (*right*) in WT and β_3 nulls as a function of age. Each point represents the mean and S.E.M. for animals at that age. The value for each animal is the summed area of 4-5 successive 70μm thick sections through the middle of dLGN. *D.* Mean and S.E.M. of the spatial extent of projections across age. The spatial extent of the ipsilateral projections (I), as well as the degree of overlap between the two eyes (O) is larger in β_3 nulls than in WTs. *E.* The averaged distribution of the log ratio (R-value) for pixel intensities of contralateral and ipsilateral eye projections at P17 and P28 for WT and β_3 nulls. A value of –2 indicates a pixel in which the contralateral signal was 100 times brighter than the ipsilateral signal; a value of zero indicates a pixel in which the contralateral signal had the same intensity as the ipsilateral signal. While WTs show a developmental decrease in equal intensity pixels, β_3 nulls remain un-segregated as late as P28. *F.* Plot of the mean and S.E.M. of variance in WT and β_3 nulls as a function of age, where smaller a variance indicates more overlap between

projections. *G*. Mean and S.E.M. of variance across age. β_3 nulls have smaller variances over all ages than WTs do, indicating less eye-specific segregation. β_3 null and (WT) dLGNs: P11 ipsilateral (i): 15 (4); overlap (o): 11 (4); variance (v): 5 (4); P14 i: 11 (14); o: 11 (8); v: 5 (4); P17 i: 7 (6); o: 6 (6); v: 5 (5); P21 i: 9 (5); o: 8 (5); v: 5 (6); P28 i: 11 (6); o: 9 (6); v: 6 (6).

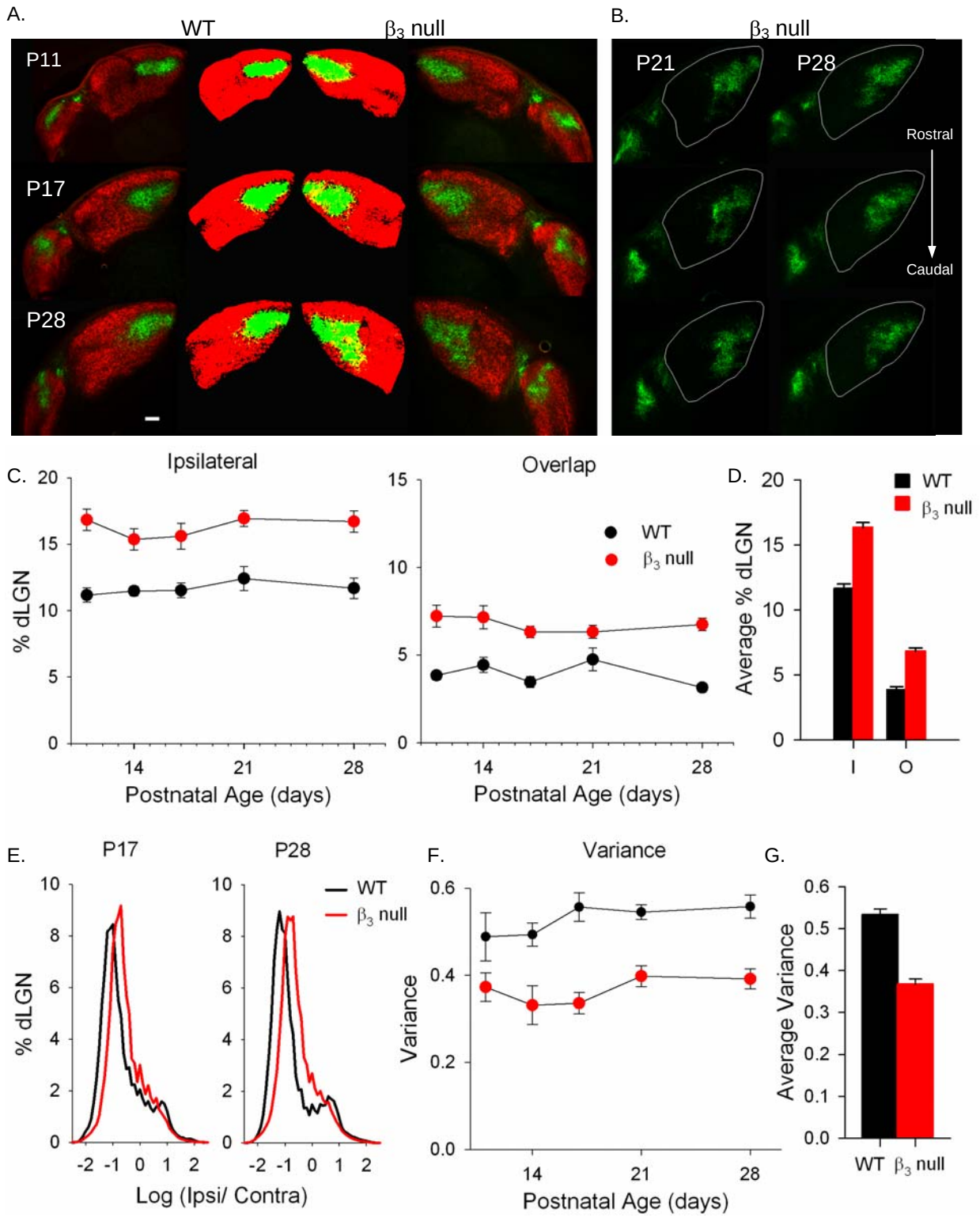

Figure 2.6

Estimates of retinal convergence in WTs and β_3 nulls: synaptic responses and stimulus intensity plots.

Representative examples of retinal convergence at different postnatal ages in WT (*left*) and β_3 null (*right*) dLGN cells. For each cell, synaptic responses are evoked by a single pulse delivered to the OT. Responses to progressive increases in stimulus intensity are shown (inset), along with corresponding amplitude by stimulus intensity plots. Each point depicts the peak amplitude of a single response, with a minimum of five responses recorded at each stimulus intensity. The horizontal numbered lines reflect the threshold between retinal inputs (see Methods). Estimates are obtained in current clamp (rows 1, 2 and 4) or in voltage clamp mode (row 3). dLGN cells in WTs show pruning of functional retinal inputs with age, while β_3 null dLGN cells retain more inputs and show less pruning than age-matched WTs. Estimates WT: P7=7, P11=5, P17=3, P21=2; β_3 null: P8=12, P12=8, P16=5, P21=7. Current clamp responses recorded at –60mV, voltage clamp at –70 and +40mV.

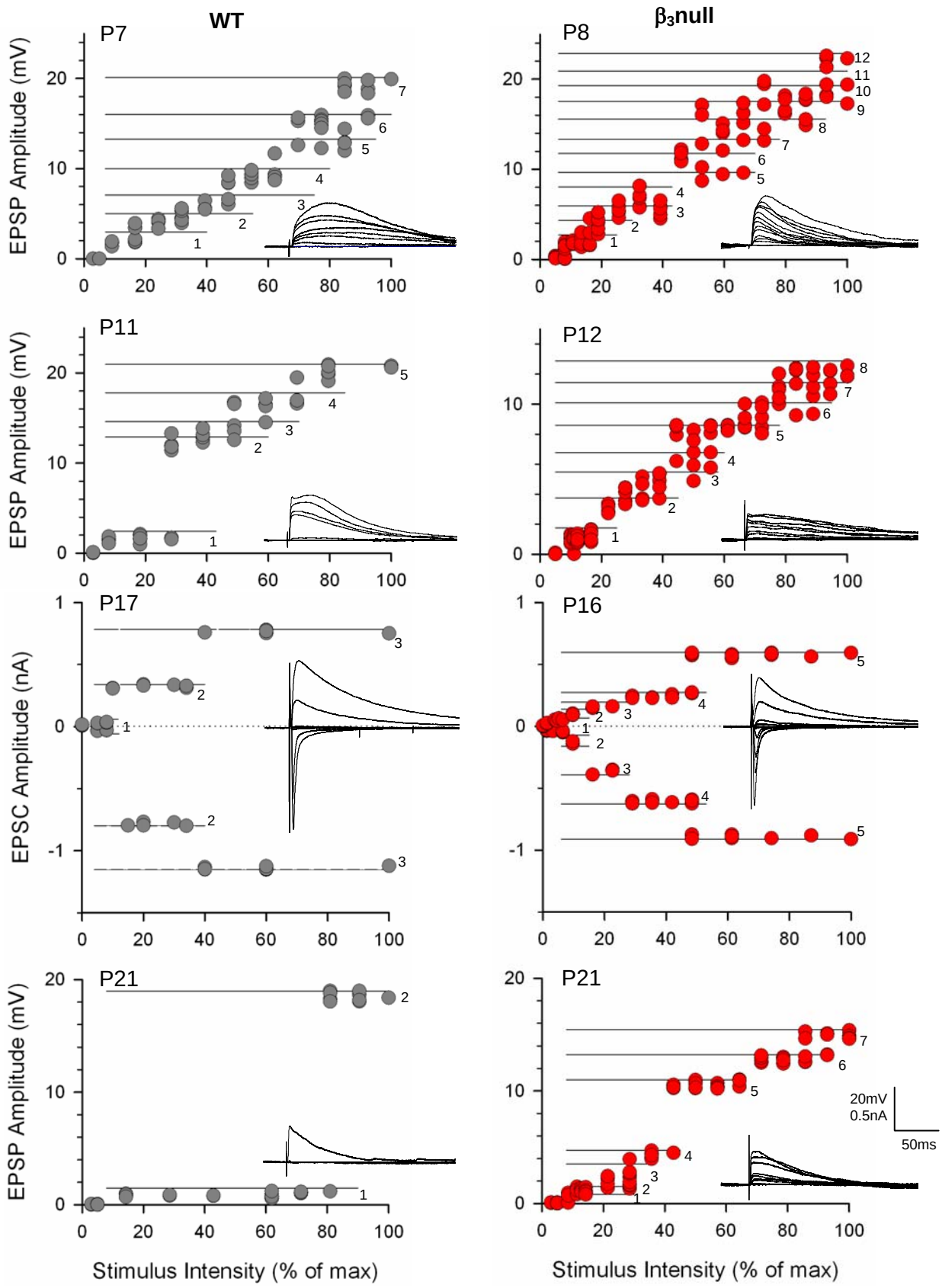

Figure 2.7

Estimates of retinal convergence in WTs and β_3 nulls: summary.

A. Plot showing number of inputs by age for WTs (*left*) and β_3 nulls (*right*). The size of each dot is proportional to the number of cells that had the same number of inputs: the smallest dots represent a single cell, the largest dot 5 cells and intermediate sized dots represent 2-4 cells. Data is fit to a single exponentials (black and red lines). Although both groups show pruning with age, β_3 nulls have cells with more inputs than age-matched WT cells do throughout development. *B.* Mean and S.E.M. of numbers of inputs by age. β_3 nulls have significantly more inputs at P7-9, P10-12 and at P16 and above. β_3 null and (WT) cells: P7-9: 5 (9); P10-12: 11 (22); P13-15: 22 (18); P16+: 31 (29).

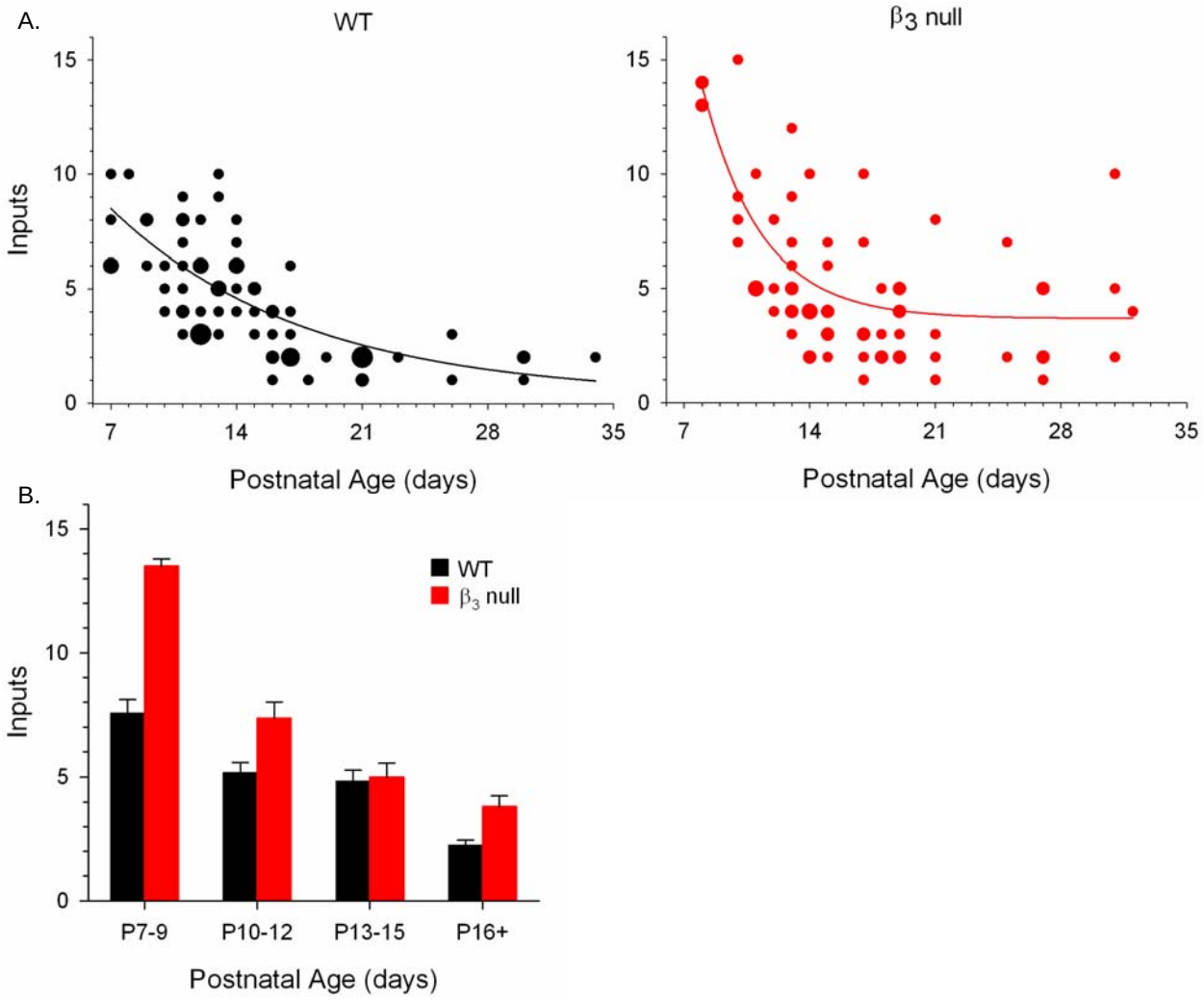

Discussion

Our results in β_3 nulls indicate that L-type Ca^{2+} channel activity, in the form of plateau potentials, plays an important role in the refinement of the retinogeniculate pathway. These mice show a greatly reduced expression of L-type Ca^{2+} channels and plateau activity (Dilger *et al*., submitted). Indeed, such a loss leads to a breakdown in eye-specific segregation and the pruning of retinal connections onto dLGN cells. We also show that the lack of the β_3 subunit has no effect on the development of AMPA or NMDA receptor mediated currents, the development of inhibitory connectivity, or on intrinsic membrane properties of dLGN cells (Dilger *et al*., submitted). Additionally, multi-electrode array recordings of whole mount retinal explants reveal that both cholinergic stage II (P7) and glutamatergic stage III (P12) retinal waves are indistinguishable from normal. These mutants also show an ERG b-wave (Ball *et al*., 2002), suggesting that the transition from retinal waves to light responses occurs normally.

The loss of the β_3 subunit leads to reduced channel expression (Birnbaumer *et al*., 1998; Dolphin, 2003) and, as reported in isolated dorsal root ganglion cells, a 60% decrease in L-type Ca^{2+} current (Namkung *et al*., 1998; Murakami *et al*., 2002). In dLGN, we too report a reduced L-type channel expression (Dilger *et al*., submitted) and while we have yet to examine the L-type current directly in the dLGN of these mutants, such a loss of expression leads to a greatly reduced incidence of plateau potentials (Dilger *et al*., submitted; Fig 2.1). Even at early postnatal ages, a time when the incidence of plateau potentials is at its peak in WT, they are only rarely observed, even when high rates of OT stimulation are used. While rare, the plateau potentials that were recorded also displayed smaller amplitudes, slower rates of rise, and increased decay times, suggesting that the associated Ca^{2+} influx occurring during these events was also greatly reduced. Perhaps these defects are expected since β subunits are known to affect many aspects

of L-type Ca^{2+} channel kinetics including channel open time, rate of channel activation and inactivation, and voltage dependency (Dolphin, 2003). Another possibility is that WT plateau potentials have a positive feedback loop in which the initial activation of L-type Ca^{2+} channels depolarizes the cell, thereby activating more L-type channels (Kammermeier & Jones, 1997). In β_3 null mice, the reduced L-type expression limits the membrane depolarization, thereby decreasing both the rate of rise and the amplitude of plateau potentials, as well as the resulting Ca^{2+} influx.

It is important to note that the lack of L-type Ca^{2+} plateau potentials affects both coarse (e.g., anatomical eye-specific segregation and the initial pruning of retinal inputs) and fine scale (e.g., continued loss of retinal inputs) phases of retinogeniculate refinement. Initially in WTs, projections from the two eyes are diffuse and overlapping but after the first postnatal week eye-specific modules form and become well organized into non-overlapping domains (Jaubert-Miazza *et al*., 2005; Muir-Robinson *et al*., 2002). In the present study, we noted that at P11 ipsilateral eye domains occupied only a small portion of dLGN territory and showed little overlap. However, in β_3 nulls, eye-specific domains never seem to develop properly. Even as late as P28, mutants had greatly expanded ipsilateral eye patches with a spatial extent that overlapped contralateral eye projections.

In WTs, coarse scale anatomical changes occurring in dLGN are also accompanied by a remodeling of functional connections. Estimates of retinal convergence reveal that at early postnatal ages, dLGN cells receive binocular input from as many as 10-12 retinal ganglion cells (Chen & Regehr, 2000; Lo *et al*., 2002; Jaubert-Miazza *et al*., 2005; Hooks & Chen, 2006). During the first few postnatal weeks, substantial pruning occurs such that dLGN cells typically end up receiving monocular input from 1-3 RGCs. Our estimates of retinal pruning are consistent

with previous reports; at P7-9 dLGN cells receive on average 8 inputs and by P16 or later average 2. In β_3 nulls, pruning is greatly impaired. At the time of our earliest recordings (P7-9) dLGN cells received on average almost twice as many inputs (14) than their WT counterparts. This defect persisted and even by P16 or later dLGN cells received twice as many inputs on average (4) as WTs.

Finally, it is important to note that retinogeniculate refinement was greatly impaired but not completely absent in β_3 nulls. While the reason for this is not entirely clear, perhaps the fact that these mutants still maintain some, albeit greatly reduced, L-type Ca^{2+} channels and plateau potentials (Dilger *et al*,, submitted) allows for a limited degree of remodeling to take place. Another possibility is that the activity-dependent influx of Ca^{2+} from other sources such as NMDA receptors (Mooney *et al*., 1993) could help offset the severity of defects produced by the loss of L-type Ca^{2+}channels and plateau activity (but see Smetters *et al*., 1994).

Perhaps the most remarkable aspect of these results is that the defects in retinogeniculate refinement occurred despite the presence of normal retinal activity. Indeed, β_3 nulls displayed stage II and III waves that were indistinguishable from normal. A number of investigators have shown that the spatial and temporal patterning of waves, as well as the inherent bursting occurring within waves is needed for both the induction of eye-specific domains as wells as their continued maintenance (Muir-Robinson *et al*., 2002; Demas *et al*., 2006). However, what has been lacking is an understanding of the underlying postsynaptic mechanisms. To our knowledge, this study is the first to isolate a potential post-synaptic substrate in the form of L-type mediated plateau potentials. Retinal waves generate robust post-synaptic activity in developing dLGN cells that has sufficient depolarization to activate L-type Ca^{2+} channels. Indeed, in an *in vitro* mouse preparation where the two eyes and retinal inputs to dLGN remain intact, retinal waves recorded

in OT appear to evoke plateau-like depolarizations in dLGN cells (Mooney *et al*., 1996). Moreover, repetitive OT stimulation in a manner that approximates retinal waves also evokes L-type Ca^{2+} channel mediated plateau potentials (Lo *et al*., 2002; Dilger *et al*., submitted). In β_3 nulls, while the strong pre-synaptic excitatory drive provided by waves appears to be intact, the apparent defects in L-type Ca^{2+} channel expression and function lead to a failure in plateau potential activation.

The impaired refinement noted in β_3 nulls are not likely due to alterations in post-synaptic glutamatergic responses, since the ratio of AMPA to NMDA receptor currents, as well as NMDAR decay times mature properly. Nonetheless, these alterations could be due to a disruption of other high threshold Ca^{2+} channels. Although at the retinogeniculate synapse, L-type Ca^{2+} channels are located post-synaptically on dLGN relay cell dendrites, other high threshold Ca^{2+} channels do contribute to the pre-synaptic vesicle release of glutamate. A reduction in these currents could lead to depolarizations that are insufficient to activate post-synaptic L-type Ca^{2+} channels and plateau activity. Previous work in β_3 nulls has found reduced N-type currents (Namkung *et al*., 1998; Murakami *et al*., 2002; Shiraiwa *et al*., 2007); however, the P/Q type which typically dominates at pre-synapses in the central nervous system (Catterall & Few, 2008) was not reduced and was, in fact, activated at less depolarized levels, making activation of these currents easier (Namkung *et al*., 1998). Since β_3 nulls have maximal NMDAR and AMPAR currents similar to age-matched WTs, we do not think that the lack of the plateau potential in these mice is a result of pre-synaptic deficits in vesicle release.

A role for the activity-dependent activation of L-type Ca^{2+} channels is consistent with a proposed Hebbian-type model of dLGN synaptic plasticity in which co-incident bursting of neighboring RGCs serves to strengthen participating retinogeniculate synapses, while

uncorrelated firing weakens others (Butts *et al*., 2007). Additionally, Ca^{2+} influx through L-type Ca^{2+} channels has been implicated in long-term changes in the synaptic strength of dLGN retinal inputs (Ziburkus *et al*., 2009). The large Ca^{2+} influx during plateau activity, as well as the association of L-type Ca^{2+} channels with CaM (Morad & Soldatov, 2005) makes the plateau potential event well suited for the implementation of refinement. CaM activation can lead to the phosphorylation of CaM kinases (CaMK), which autophosphorylate during high Ca^{2+} levels, leading to sustained activation and signaling cascades to initiate the transcription of plasticity related genes. In fact, CREB, a CaMK activated transcription factor, has been shown to have a window of high expression and activation at the peak of retinogeniculate refinement (Pham *et al*., 2001). The link between these signaling cascades and L-type activity could also help explain the lack of retinogeniculate refinement in a mouse with mutant CREB (Pham *et al*., 2001). While a direct relationship between plateau activity and the activation of CREB or other signaling molecules is presently lacking, future experiments that make use of β_3 nulls may offer a means to explore such avenues.

Conclusion

Our results indicate that L-type Ca^{2+} channel activity in the form of synaptically evoked plateau potentials, is regulated by a number of factors at early postnatal development including spatial and temporal summation, the degree of retinogeniculate convergence, intrinsic feed-forward inhibitory responses and the expression of the L-type Ca^{2+} channel. Moreover, we have identified that such activity is necessary for refinement, both in terms of eye-specific segregation and pruning of retinal inputs onto dLGN relay cells. Figure 3.1 presents a scenario by which early retinal activity can lead to the refinement of retinogeniculate projections and connections. At early ages, waves propagate across the retina and drive robust post-synaptic activity in dLGN cells (Mooney *et al*., 1996). At these times, the projections are diffuse and individual cells receive binocular input from several RGCs (Fig. 3.1A-B; Jaubert-Miazza *et al*., 2005; Ziburkus & Guido, 2006). Coincident wave activity in multiple neighboring RGCs which project to the same dLGN cell leads to spatial and temporal summation and evoke long lasting depolarizations. These depolarizations, left unchecked by feed-forward inhibition, provide the amplitude and duration necessary to evoke L-type Ca^{2+} channels and plateau activity. In addition, high expression of L-type Ca^{2+} channels as well as their somatodendritic positioning in close

proximity to retinal terminals further promotes plateau activity. Pharmacology experiments reveal that plateau potentials are mediated exclusively by the L-type Ca^{2+} channel. Bath application of the NMDAR antagonist APV or the intracellular use of the Ca^{2+} chelator BAPTA had no effect on plateau activity (Fig. 1.2). Plateau potentials would allow for a huge Ca^{2+} influx into the cell, a potent signal for the transcription of plasticity related genes and retinogeniculate refinement.

At older ages, around natural eye opening, retinal waves cease and are replaced by visually evoked activity (Fig. 3.1D). At this time, the majority of refinement is complete, and post-synaptic events in dLGN cells are comprised of fast excitatory events (AMPA and NMDA) and intrinsic inhibitory activity. Additionally, L-type Ca^{2+} channel expression is much lower, and plateau activity is rare. It is important to note that while plateau potentials are infrequent, L-type Ca^{2+} channel activity is still prevalent in the adult animal where it helps to regulate overall cellular excitability and response mode (Kammermeir & Jones, 1997; Zhou *et al*., 1997; Pape *et al*., 2004).

In the β_3 null mouse, the low expression of L-type Ca^{2+} channels greatly limits the incidence of plateau potentials, even though the retinal waves and dLGN excitatory synaptic responses are normal. The few we observed required high levels of stimulation and were kinetically different from WT plateaus, in a way that seems to restrict high Ca^{2+} influx and limit refinement. It has been reported in the developing visual cortex that the removal or reduction of NMDAR subunits impairs activity-dependent elimination of synapses (Cho *et al*., 2009). Indeed, a similar scenario seems to occur in β_3 null mice in which activity dependent remodeling is lacking.

Thus, these studies reveal a potential substrate for retinogeniculate refinement in the form

of L-type Ca^{2+} channel plateau activity. A likely instructive rule which could implement activity-dependant changes is a Hebbian type-learning model of synaptic plasticity (burst-time dependent plasticity [BTDP]), based on the relative timing between bursts of action potentials in RGCs and their ability to evoke high amplitude activity in dLGN cells (Butts *et al*., 2007). In this model, bidirectional changes in synaptic strength are the mechanism by which some synapses are strengthened and maintained while others are weakened and eliminated. During a retinal wave, neighboring RGCs that project onto the same dLGN cell burst synchronously (Fig. 3.1A). These inputs are strengthened, whereas non-neighboring RGCs, while firing spontaneously, do not participate in the same temporally correlated wave. As a result, their activity is not coincident with the other inputs and they fail to evoke plateau potentials, leading to synapse weakening. Indeed, we were never able to evoke plateau activity with high frequency stimulation of a single fiber, even at early ages (data not shown). As waves grow weaker and shorter (during glutamatergic phase III), fewer RGCs participate, leading to a more focal form of strengthening and elimination. The BTDP model depends on the concomitant activity of pre- and post-synaptic elements. In β_3 nulls, while the pre-synaptic activity is unimpaired, the post-synaptic event (L-type plateau potentials) is altered, and there is a lack of refinement.

What remains unknown is the mechanism by which certain synapses are tagged to be strengthened and maintained while others are eliminated. At early postnatal ages a single dLGN relay cell dendrite may contain inputs from both the ipsilateral and contralateral eye, but in the adult relay cells receive only monocular input (Ziburkus & Guido, 2006). Additionally, inputs from the same eye, which are potentially in close proximity on the dendrite, are also selectively pruned. Furthermore, based on preliminary studies in our lab we know that there is a proximal to distal gradient of retinal inputs, but that pruning seems to occur uniformly throughout the

dendritic tree and does not target one specific region. However, long-term changes in synaptic function require the nuclear transcription, synthesis and trafficking of activity-induced gene products (Cohen & Greenberg, 2008). How the decision to maintain and strengthen or weaken and eliminate individual inputs is located back to a single segment of the dendrite is still unidentified.

One idea that has been proposed in recent years is the role of the immune system in synapse elimination. This model, initially proposed in the developing neuromuscular junction, involves the expression of two types of signals from synapses with strong activity: a short-range protective signal to protect "self" and a longer-range, diffusible punishment signal to tag nearby weak synapses for elimination by phagocytosis via microglia (Jennings, 1994; Schafer & Stevens, 2010). In fact, recent work has identified some immune system molecules that could be involved in activity-dependent synapse elimination and are necessary for proper eye-specific segregation. One of these is major histocompatability complex class 1 (MHC1), a large family of immune genes (Fig. 3.1C). Signaling through MHC1 is inhibited by depolarization (Boulanger *et al*., 2001), and since MHC1 is thought to be located in the post-synapse (Datwani *et al*., 2010), those that are less-active may be targeted for removal via MHC1 activation (Boulanger *et al*., 2001). Other immune molecules (components of the complement cascade and neuronal pentraxins) have also been implicated in fine-scale synaptic pruning of retinal inputs (Stevens *et al*., 2007) and glutamate receptor insertion at retinogeniculate synapses (Koch & Ullian, 2010), although it is unclear exactly how they are activated and what signaling pathways they affect (Schafer & Stevens, 2010), they do have interesting implications. For instance, the lack of high amplitude post-synaptic depolarizations in β_3 nulls could lead to a reduction in synapse elimination via some of these mechanisms.

Another possibility is interactions with the cytoskeleton architecture. Spines, the small protrusions from dendritic shafts that are the primary postsynaptic location of excitatory synapses in the CNS and constitute calcium microdomains (Blackstone & Sheng, 2002), are highly motile due to their microfilament scaffolding of polymerized actin molecules. Cellular signaling can dictate spine morphology in an activity dependent manner by tightly regulating the assembly and disassembly of these long, thin fibers (Oertner & Matus, 2004). The actin cytoskeleton also helps to traffic and anchor proteins such as post-synaptic receptors, so changes in actin polymerization have the added potential of directly influencing synaptic function and strength (Bloodgood & Sabatini, 2007). Cofilin is an actin binding protein that depolymerizes and reorganizes actin filaments (Huang *et al*., 2006). Ca^{2+} influx can activate calcineurin (CaN), a Ca^{2+}/CaM-dependent phosphatase important in visual plasticity (Yang *et al*., 2005), which, through a cascade of events, causes the dephosphorylation of cofilin (Fig. 3.1C; Huang *et al*., 2006). This activates cofilin to bind and sever actin filaments. Numerous studies have implicated cofilin in neuronal activity dependent plasticity, including the remodeling of dendritic spines and the elimination of synaptic connections (Zhou *et al*., 2004).

However, mouse dLGN relay cells do not appear to have spines (Rafols & Valverde, 1973; Bickford *et al*., 2010). Instead, they are studded with small 'dendritic protrusions' that are morphologically distinct from dendritic spines. While specific inquires into the function of these protrusions in relation to activity dependent, input specific plasticity and signaling have not been directly addressed, other studies have found both synapse specific plasticity and Ca^{2+} microdomains in aspiny cells (Goldberg *et al*., 2003; Lamsa *et al*., 2005; Soler-Llavina & Sabatini, 2006). Furthermore, there is evidence of small Ca^{2+} microdomains at the mouth of channels either via direct interaction of proteins with channels or through localization of the

channels and effector proteins within the actin cytoskeleton, which could help signal and direct specificity (Cavazzini *et al*., 2005).

Additionally unknown are the underlying intracellular signaling cascades are responsible for implementing changes in synaptic strength. One candidate for an intracellular effector that can be initiated by fluctuations in Ca^{2+} levels is calmodulin. The carboxyl terminus of the L-type Ca^{2+} channel has been shown to directly interact with this Ca^{2+} modulated protein (Morad & Soldatv, 2005), which can then regulate various protein targets. One of the major targets of CaM is the Ca^{2+}/CaM-dependent kinase CaMKII, a temporally sensitive signaling molecule. With low frequency Ca^{2+} influxes, CaMKII is deactivated completely between pulses, whereas with high frequency stimulation, the continued presence of Ca^{2+} and activated CaM permits CaMKII autophosphorylation, allowing for maintained maximal activation even after Ca^{2+} levels return to baseline (Cavazzni *et al*., 2005). This scenario might be especially possible given our model of high-amplitude, long-lasting and slow decaying depolarization plateau potentials.

What is the link between CaM and CaMKII and transcription? The transcription factor CREB often serves as the prototype for Ca^{2+}-dependent regulation of transcription, and has been implicated in eye-specific refinement (Pham *et al*., 2001). When phosphorylated CREB enters the nucleus where it can initiate the transcription of genes with CREB binding sites (CREs) within its promoter region (Lonze & Ginty, 2002). Additionally, Ca^{2+} influx specifically through L-type Ca^{2+} channels has been shown to support CREB-dependent transcription (Moosmang et al, 2005b). However, when we looked at CREB and phosphorylated CREB levels in WT and β_3 null mice using a variety of methods (western blot with chemiluminescence and Odyssey Imaging System, ELISA), the results were variable and ambiguous (data not shown). There are a number of factors that could contribute to this. CREB is such a ubiquitous transcription factor

used by the cell to regulate many divergent outcomes and a number of different signaling pathways lead to its phosphorylation, indicating that there are many mechanisms involved in the regulation of CREB activity (Cohen & Greenberg, 2008). Therefore, moment-to-moment fluctuations in Ca^{2+} levels due to a variety of commonplace cellular activities may cloud results.

In addition to CREB, a number of other transcription factors have been shown to be dependent on Ca^{2+} fluxes through the L-type Ca^{2+} channel and CaM. One of those is the myocyte enhancer factor 2 (MEF2; Dolmetsch *et al*., 2001). Like CREB, MEF2 can be regulated by neuronal activity and Ca^{2+} levels, can mediate experience-dependent development and likely depends coordinate cellular regulation (Cohen & Greenberg, 2008). However, there is a range of other possibilities as well (NFAT [nuclear factor of activated T-cells, a transcription factor initially discovered in the immune system but known to control CNS processes as well]; MeCP2 [methyl cytosine-guanine binding protein, which plays a role in condensing and silencing specific DNA transcription sites]; CREST [Ca^{2+} responsive transcriptional co-activator, involved in dendritic growth and morphology], etc), and how these are controlled and coordinated with CREB is largely unknown.

However, this raises the issue of Ca^{2+} signaling specificity: how can one signal have two opposite effects? The simplest model is based on the greater affinity of Ca^{2+} for phosphatases than kinases: low levels of Ca^{2+} trigger phosphatases and the initiation of dephosphorylation and weakening events, whereas higher levels activate kinases and lead to the phosphorylation of another set of effector proteins, leading to synapse strengthening (Fig. 3.1C; Cavazzini *et al*., 2005). In fact, it has been shown that high amplitude Ca^{2+} influxes lead to potentiation, while smaller signals lead to depression (Ismailov *et al*., 2004). The Ca^{2+} levels necessary to activate CaMKII might only be reached within Ca^{2+} microdomains in a dendritic spine or near the mouth

of the channel, increasing the likelihood for synapse specificity (Cavazzini *et al*., 2005). Additionally, phosphatases triggered in response to protocols leading to depression also dephosphorylate CaMKII, preventing the two conflicting signals from cascading at once (Cavazzini *et al*., 2005).

While our studies have isolated an event that can implement high levels of Ca^{2+} influx, the challenges that lie ahead are to link this Ca^{2+} to pathways that are able to signal and traffic gene products back to specific sites and synapses to implement long-term changes in synaptic plasticity and eventually lead to the activity-dependent retinogeniculate refinement.

Figure 3.1

Potential mechanisms underlying activity-dependent refinement in dLGN.

A. Spike trains and retinal location of six RGCs that project onto a single relay cell in dLGN (*B*). During coarse scale refinement, waves in neighboring RGCs fire synchronously, while activity of more disparate cells or cells from the other eye fire at different times (asynchronously). A wave leads to co-incident activity in the four red RCGs, and evokes a plateau potential in the relay cell. Activity from the RCG in the ipsilateral eye (green) and the non-neighboring, same eye RGC (purple) does not sufficiently depolarize the cell to activate L-type Ca^{2+} channel activity. *C.* Proposed mechanisms for the underlying signaling cascades and site specific changes in post-synaptic strength. Strong depolarization at red post-synaptic sites inhibits MHC1 signaling, thereby precenting microglial attack. Purple and green synapses, however, remain vulnerable. High Ca^{2+} influx (red synapses) activates kinases leading to the transcription and trafficking of plasticity related proteins that could potentially lead to a strucutal change at targeted post-synaptic sites (e.g. AMPR insertion). Low Ca^{2+} levels (purple and green synapses) activate phosphatases, which can lead to the activation of cofilin to depolymerize actin filaments (blue dots). *D.* During fine scale refinement, waves are smaller and have fewer participating RGCs, leading to additional pruning and strengthening of remaining synapses. Eventually, adult-like patterns of connectivity are established. These are comprised of 1-3 monocular inputs and give rise to large EPSPs.

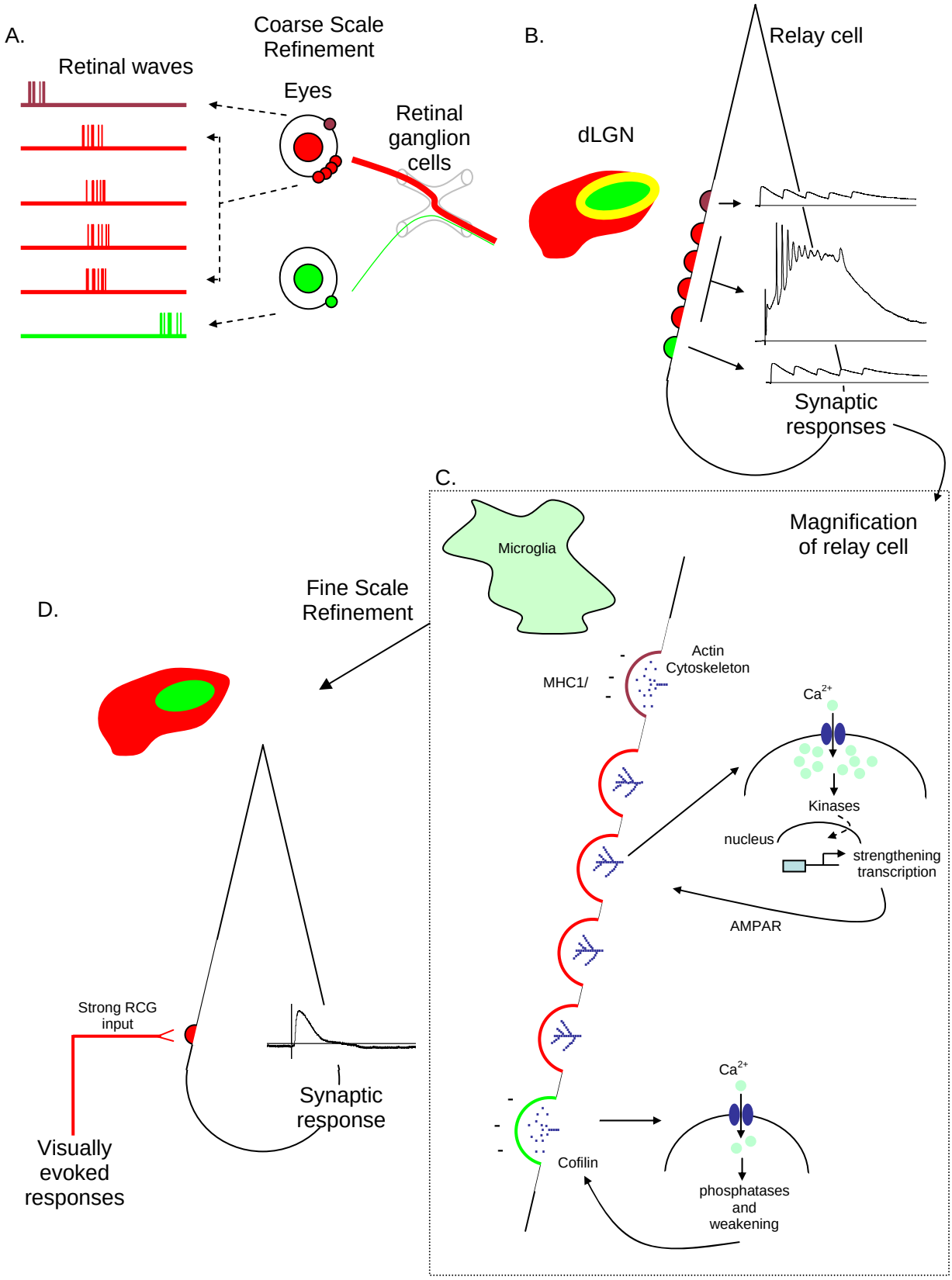

References

Ball, SL, Powers, PA, Shin, HS, Morgans, CW, Peachey, NS & Gregg, RG (2002). Role of the beta(2) subunit of voltage-dependent calcium channels in the retinal outer plexiform layer. *Invest Ophthalmol Vis Sci* 5, 1595-1603.

Bansal, A, Singer, JH, Hwang, BJ, Xu, W, Beaudet, A & Feller, MB (2000). Mice lacking specific nicotinic acetylcholine receptor subunits exhibit dramatically altered spontaneous activity patterns and reveal a limited role for retinal waves in forming ON and OFF circuits in the inner retina. *J Neurosci* 20, 7672-7681.

Bardo, S, Cavazzini, MG & Emptage, N (2006). The role of the endoplasmic reticulum Ca2+ store in the plasticity of central neurons. *Trends Pharmacol Sci* 2, 78-84, DOI: 10.1016/j.tips.2005.12.008.

Berridge, MJ, Lipp, P & Bootman, MD (2000). The versatility and universality of calcium signalling. *Nat Rev Mol Cell Biol* 1, 11-21, DOI: 10.1038/35036035.

Bichet, D, Cornet, V, Geib, S, Carlier, E, Volsen, S, Hoshi, T, Mori, Y & De Waard, M (2000). The I-II loop of the Ca2+ channel alpha1 subunit contains an endoplasmic reticulum retention signal antagonized by the beta subunit. *Neuron* 1, 177-190.

Bickford, ME, Slusarczyk, A, Dilger, EK, Krahe, TE, Kucuk, C & Guido, W (2010). Synaptic development of the mouse dorsal lateral geniculate nucleus. *J Comp Neurol* 5, 622-635, DOI: 10.1002/cne.22223.

Birnbaumer, L, Qin, N, Olcese, R, Tareilus, E, Platano, D, Costantin, J & Stefani, E (1998). Structures and functions of calcium channel beta subunits. *J Bioenerg Biomembr* 4, 357-375.

Blackstone, C & Sheng, M (2002). Postsynaptic calcium signaling microdomains in neurons. *Front Biosci*, d872-85.

Blitz, DM & Regehr, WG (2005). Timing and specificity of feed-forward inhibition within the LGN. *Neuron* 6, 917-928, DOI: 10.1016/j.neuron.2005.01.033.

Bloodgood, BL & Sabatini, BL (2007). Ca(2+) signaling in dendritic spines. *Curr Opin Neurobiol* 3, 345-351, DOI: 10.1016/j.conb.2007.04.003.

Budde, T, Meuth, S & Pape, HC (2002). Calcium-dependent inactivation of neuronal calcium channels. *Nat Rev Neurosci* 11, 873-883, DOI: 10.1038/nrn959.

Budde, T, Munsch, T & Pape, HC (1998). Distribution of L-type calcium channels in rat thalamic neurones. *Eur J Neurosci* 2, 586-597.

Butts, DA, Kanold, PO & Shatz, CJ (2007). A burst-based "Hebbian" learning rule at retinogeniculate synapses links retinal waves to activity-dependent refinement. *PLoS Biol* 3, e61, DOI: 10.1371/journal.pbio.0050061.

Catterall, WA & Few, AP (2008). Calcium channel regulation and presynaptic plasticity. *Neuron* 6, 882-901, DOI: 10.1016/j.neuron.2008.09.005.

Catterall, WA, Perez-Reyes, E, Snutch, TP & Striessnig, J (2005). International Union of Pharmacology. XLVIII. Nomenclature and structure-function relationships of voltage-gated calcium channels. *Pharmacol Rev* 4, 411-425, DOI: 10.1124/pr.57.4.5.

Cavazzini, M, Bliss, T & Emptage, N (2005). Ca2+ and synaptic plasticity. *Cell Calcium* 3-4, 355-367, DOI: 10.1016/j.ceca.2005.06.013.

Chen, C & Regehr, WG (2000). Developmental remodeling of the retinogeniculate synapse. *Neuron* 3, 955-966.

Cho, KK, Khibnik, L, Philpot, BD & Bear, MF (2009). The ratio of NR2A/B NMDA receptor subunits determines the qualities of ocular dominance plasticity in visual cortex. *Proc Natl Acad Sci U S A* 13, 5377-5382, DOI: 10.1073/pnas.0808104106.

Cohen, S & Greenberg, ME (2008). Communication between the synapse and the nucleus in neuronal development, plasticity, and disease. *Annu Rev Cell Dev Biol*, 183-209, DOI: 10.1146/annurev.cellbio.24.110707.175235.

Corlew, R, Bosma, MM & Moody, WJ (2004). Spontaneous, synchronous electrical activity in neonatal mouse cortical neurones. *J Physiol* Pt 2, 377-390, DOI: 10.1113/jphysiol.2004.071621.

Crepel, V, Aronov, D, Jorquera, I, Represa, A, Ben-Ari, Y & Cossart, R (2007). A parturition-associated nonsynaptic coherent activity pattern in the developing hippocampus. *Neuron* 1, 105-120, DOI: 10.1016/j.neuron.2007.03.007.

Crunelli, V, Haby, M, Jassik-Gerschenfeld, D, Leresche, N & Pirchio, M (1988). Cl– - and K+-dependent inhibitory postsynaptic potentials evoked by interneurones of the rat lateral geniculate nucleus. *J Physiol*, 153-176.

Datwani, A, McConnell, MJ, Kanold, PO, Micheva, KD, Busse, B, Shamloo, M, Smith, SJ & Shatz, CJ (2009). Classical MHCI molecules regulate retinogeniculate refinement and limit ocular dominance plasticity. *Neuron* 4, 463-470, DOI: 10.1016/j.neuron.2009.10.015.

Demas, J, Eglen, SJ & Wong, RO (2003). Developmental loss of synchronous spontaneous activity in the mouse retina is independent of visual experience. *J Neurosci* 7, 2851-2860.

Demas, J, Sagdullaev, BT, Green, E, Jaubert-Miazza, L, McCall, MA, Gregg, RG, Wong, RO & Guido, W (2006). Failure to maintain eye-specific segregation in nob, a mutant with abnormally patterned retinal activity. *Neuron* 2, 247-259, DOI: 10.1016/j.neuron.2006.03.033.

Dietrich, D, Kirschstein, T, Kukley, M, Pereverzev, A, von der Brelie, C, Schneider, T & Beck, H (2003). Functional specialization of presynaptic Cav2.3 Ca2+ channels. *Neuron* 3, 483-496.

Dolmetsch, RE, Pajvani, U, Fife, K, Spotts, JM & Greenberg, ME (2001). Signaling to the nucleus by an L-type calcium channel-calmodulin complex through the MAP kinase pathway. *Science* 5541, 333-339, DOI: 10.1126/science.1063395.

Dolphin, AC (2003). Beta subunits of voltage-gated calcium channels. *J Bioenerg Biomembr* 6, 599-620.

Goldberg, JH, Tamas, G, Aronov, D & Yuste, R (2003). Calcium microdomains in aspiny dendrites. *Neuron* 4, 807-821.

Greer, PL & Greenberg, ME (2008). From synapse to nucleus: calcium-dependent gene transcription in the control of synapse development and function. *Neuron* 6, 846-860, DOI: 10.1016/j.neuron.2008.09.002.

Gregg, RG, Messing, A, Strube, C, Beurg, M, Moss, R, Behan, M, Sukhareva, M, Haynes, S, Powell, JA, Coronado, R & Powers, PA (1996). Absence of the beta subunit (cchb1) of the skeletal muscle dihydropyridine receptor alters expression of the alpha 1 subunit and eliminates excitation-contraction coupling. *Proc Natl Acad Sci U S A* 24, 13961-13966.

Guido, W (2008). Refinement of the retinogeniculate pathway. *J Physiol*, DOI: 10.1113/jphysiol.2008.157115.

Guido, W, Lo, FS & Erzurumlu, RS (2001). Synaptic plasticity in the trigeminal principal nucleus during the period of barrelette formation and consolidation. *Brain Res Dev Brain Res* 1, 97-102.

Hernandez-Cruz, A & Pape, HC (1989). Identification of two calcium currents in acutely dissociated neurons from the rat lateral geniculate nucleus. *J Neurophysiol* 6, 1270-1283.

Hooks, BM & Chen, C (2006). Distinct roles for spontaneous and visual activity in remodeling of the retinogeniculate synapse. *Neuron* 2, 281-291, DOI: 10.1016/j.neuron.2006.07.007.

Huang, TY, DerMardirossian, C & Bokoch, GM (2006). Cofilin phosphatases and regulation of actin dynamics. *Curr Opin Cell Biol* 1, 26-31, DOI: 10.1016/j.ceb.2005.11.005.

Huberman, AD, Feller, MB & Chapman, B (2008). Mechanisms underlying development of visual maps and receptive fields. *Annu Rev Neurosci*, 479-509, DOI: 10.1146/annurev.neuro.31.060407.125533.

Ismailov, I, Kalikulov, D, Inoue, T & Friedlander, MJ (2004). The kinetic profile of intracellular calcium predicts long-term potentiation and long-term depression. *J Neurosci* 44, 9847-9861, DOI: 10.1523/JNEUROSCI.0738-04.2004.

Jaubert-Miazza, L, Green, E, Lo, FS, Bui, K, Mills, J & Guido, W (2005). Structural and functional composition of the developing retinogeniculate pathway in the mouse. *Vis Neurosci* 5, 661-676, DOI: 10.1017/S0952523805225154.

Jennings, C (1994). Developmental neurobiology. Death of a synapse. *Nature* 6506, 498-499, DOI: 10.1038/372498a0.

Jeon, D, Song, I, Guido, W, Kim, K, Kim, E, Oh, U & Shin, HS (2008). Ablation of Ca2+ channel beta3 subunit leads to enhanced N-methyl-D-aspartate receptor-dependent long term potentiation and improved long term memory. *J Biol Chem*, DOI: 10.1074/jbc.M800816200.

Kammermeier, PJ & Jones, SW (1998). Facilitation of L-type calcium current in thalamic neurons. *J Neurophysiol* 1, 410-417.

Kammermeier, PJ & Jones, SW (1997). High-voltage-activated calcium currents in neurons acutely isolated from the ventrobasal nucleus of the rat thalamus. *J Neurophysiol* 1, 465-475.

Koch, SM & Ullian, EM (2010). Neuronal pentraxins mediate silent synapse conversion in the developing visual system. *J Neurosci* 15, 5404-5414, DOI: 10.1523/JNEUROSCI.4893-09.2010.

Kornhauser, JM, Cowan, CW, Shaywitz, AJ, Dolmetsch, RE, Griffith, EC, Hu, LS, Haddad, C, Xia, Z & Greenberg, ME (2002). CREB transcriptional activity in neurons is regulated by multiple, calcium-specific phosphorylation events. *Neuron* 2, 221-233.

Lamsa, K, Heeroma, JH & Kullmann, DM (2005). Hebbian LTP in feed-forward inhibitory interneurons and the temporal fidelity of input discrimination. *Nat Neurosci* 7, 916-924, DOI: 10.1038/nn1486.

Liljelund, P, Netzeband, JG & Gruol, DL (2000). L-Type calcium channels mediate calcium oscillations in early postnatal Purkinje neurons. *J Neurosci* 19, 7394-7403.

Liu, X & Chen, C (2008). Different roles for AMPA and NMDA receptors in transmission at the immature retinogeniculate synapse. *J Neurophysiol* 2, 629-643, DOI: 10.1152/jn.01171.2007.

Lo, FS & Erzurumlu, RS (2002). L-type calcium channel-mediated plateau potentials in barrelette cells during structural plasticity. *J Neurophysiol* 2, 794-801.

Lo, FS & Mize, RR (2000). Synaptic regulation of L-type Ca(2+) channel activity and long-term depression during refinement of the retinocollicular pathway in developing rodent superior colliculus. *J Neurosci* 3, RC58.

Lo, FS, Ziburkus, J & Guido, W (2002). Synaptic mechanisms regulating the activation of a Ca(2+)-mediated plateau potential in developing relay cells of the LGN. *J Neurophysiol* 3, 1175-1185.

Lonze, BE & Ginty, DD (2002). Function and regulation of CREB family transcription factors in the nervous system. *Neuron* 4, 605-623.

Lu, B, Wang, KH & Nose, A (2009). Molecular mechanisms underlying neural circuit formation. *Curr Opin Neurobiol* 2, 162-167, DOI: 10.1016/j.conb.2009.04.004.

MacLeod, N, Turner, C & Edgar, J (1997). Properties of developing lateral geniculate neurones in the mouse. *Int J Dev Neurosci* 2, 205-224.

Magee, JC & Johnston, D (1997). A synaptically controlled, associative signal for Hebbian plasticity in hippocampal neurons. *Science* 5297, 209-213.

Malenka, RC & Bear, MF (2004). LTP and LTD: an embarrassment of riches. *Neuron* 1, 5-21, DOI: 10.1016/j.neuron.2004.09.012.

Mermelstein, PG, Bito, H, Deisseroth, K & Tsien, RW (2000). Critical dependence of cAMP response element-binding protein phosphorylation on L-type calcium channels supports a selective response to EPSPs in preference to action potentials. *J Neurosci* 1, 266-273.

Mooney, R, Madison, DV & Shatz, CJ (1993). Enhancement of transmission at the developing retinogeniculate synapse. *Neuron* 5, 815-825.

Mooney, R, Penn, AA, Gallego, R & Shatz, CJ (1996). Thalamic relay of spontaneous retinal activity prior to vision. *Neuron* 5, 863-874.

Moosmang, S, Haider, N, Klugbauer, N, Adelsberger, H, Langwieser, N, Muller, J, Stiess, M, Marais, E, Schulla, V, Lacinova, L, Goebbels, S, Nave, KA, Storm, DR, Hofmann, F & Kleppisch, T (2005**a**). Role of hippocampal Cav1.2 Ca2+ channels in NMDA receptor-independent synaptic plasticity and spatial memory. *J Neurosci* 43, 9883-9892, DOI: 10.1523/JNEUROSCI.1531-05.2005.

Moosmang, S, Lenhardt, P, Haider, N, Hofmann, F & Wegener, JW (2005**b**). Mouse models to study L-type calcium channel function. *Pharmacol Ther* 3, 347-355, DOI: 10.1016/j.pharmthera.2004.12.003.

Morad, M & Soldatov, N (2005). Calcium channel inactivation: possible role in signal transduction and Ca2+ signaling. *Cell Calcium* 3-4, 223-231, DOI: 10.1016/j.ceca.2005.06.027.

Morisset, V & Nagy, F (1999). Ionic basis for plateau potentials in deep dorsal horn neurons of the rat spinal cord. *J Neurosci* 17, 7309-7316.

Muir-Robinson, G, Hwang, BJ & Feller, MB (2002). Retinogeniculate axons undergo eye-specific segregation in the absence of eye-specific layers. *J Neurosci* 13, 5259-5264, DOI: 20026563.

Murakami, M, Fleischmann, B, De Felipe, C, Freichel, M, Trost, C, Ludwig, A, Wissenbach, U, Schwegler, H, Hofmann, F, Hescheler, J, Flockerzi, V & Cavalie, A (2002). Pain perception in mice lacking the beta3 subunit of voltage-activated calcium channels. *J Biol Chem* 43, 40342-40351, DOI: 10.1074/jbc.M203425200.

Namkung, Y, Smith, SM, Lee, SB, Skrypnyk, NV, Kim, HL, Chin, H, Scheller, RH, Tsien, RW & Shin, HS (1998). Targeted disruption of the Ca2+ channel beta3 subunit reduces N- and L-type Ca2+ channel activity and alters the voltage-dependent activation of P/Q-type Ca2+ channels in neurons. *Proc Natl Acad Sci U S A* 20, 12010-12015.

Oertner, TG & Matus, A (2005). Calcium regulation of actin dynamics in dendritic spines. *Cell Calcium* 5, 477-482, DOI: 10.1016/j.ceca.2005.01.016.

Pape, HC, Munsch, T & Budde, T (2004). Novel vistas of calcium-mediated signalling in the thalamus. *Pflugers Arch* 2, 131-138, DOI: 10.1007/s00424-003-1234-5.

Pham, TA, Rubenstein, JL, Silva, AJ, Storm, DR & Stryker, MP (2001). The CRE/CREB pathway is transiently expressed in thalamic circuit development and contributes to refinement of retinogeniculate axons. *Neuron* 3, 409-420.

Rafols, JA & Valverde, F (1973). The structure of the dorsal lateral geniculate nucleus in the mouse. A Golgi and electron microscopic study. *J Comp Neurol* 3, 303-332, DOI: 10.1002/cne.901500305.

Rekling, JC & Feldman, JL (1997). Calcium-dependent plateau potentials in rostral ambiguus neurons in the newborn mouse brain stem in vitro. *J Neurophysiol* 5, 2483-2492.

Schafer, DP & Stevens, B (2010). Synapse elimination during development and disease: immune molecules take centre stage. *Biochem Soc Trans* 2, 476-481, DOI: 10.1042/BST0380476.

Scharfman, HE, Lu, SM, Guido, W, Adams, PR & Sherman, SM (1990). N-methyl-D-aspartate receptors contribute to excitatory postsynaptic potentials of cat lateral geniculate neurons recorded in thalamic slices. *Proc Natl Acad Sci U S A* 12, 4548-4552.

Sherman, SM & Guillery, RW (2002). The role of the thalamus in the flow of information to the cortex. *Philos Trans R Soc Lond B Biol Sci* 1428, 1695-1708, DOI: 10.1098/rstb.2002.1161.

Shiraiwa, T, Kashiwayanagi, M, Iijima, T & Murakami, M (2007). Involvement of the calcium channel beta3 subunit in olfactory signal transduction. *Biochem Biophys Res Commun* 4, 1019-1024, DOI: 10.1016/j.bbrc.2007.02.063.

Singer, JH, Mirotznik, RR & Feller, MB (2001). Potentiation of L-type calcium channels reveals nonsynaptic mechanisms that correlate spontaneous activity in the developing mammalian retina. *J Neurosci* 21, 8514-8522.

Smetters, DK, Hahm, J & Sur, M (1994). An N-methyl-D-aspartate receptor antagonist does not prevent eye-specific segregation in the ferret retinogeniculate pathway. *Brain Res* 1-2, 168-178.

Soler-Llavina, GJ & Sabatini, BL (2006). Synapse-specific plasticity and compartmentalized signaling in cerebellar stellate cells. *Nat Neurosci* 6, 798-806, DOI: 10.1038/nn1698.

Stevens, B, Allen, NJ, Vazquez, LE, Howell, GR, Christopherson, KS, Nouri, N, Micheva, KD, Mehalow, AK, Huberman, AD, Stafford, B, Sher, A, Litke, AM, Lambris, JD, Smith, SJ, John, SW & Barres, BA (2007). The classical complement cascade mediates CNS synapse elimination. *Cell* 6, 1164-1178, DOI: 10.1016/j.cell.2007.10.036.

Torborg, CL & Feller, MB (2005). Spontaneous patterned retinal activity and the refinement of retinal projections. *Prog Neurobiol* 4, 213-235, DOI: 10.1016/j.pneurobio.2005.09.002.

Torborg, CL & Feller, MB (2004). Unbiased analysis of bulk axonal segregation patterns. *J Neurosci Methods* 1-2, 17-26, DOI: 10.1016/j.jneumeth.2003.11.019.

Torborg, CL, Hansen, KA & Feller, MB (2005). High frequency, synchronized bursting drives eye-specific segregation of retinogeniculate projections. *Nat Neurosci* 1, 72-78, DOI: 10.1038/nn1376.

Yang, Y, Fischer, QS, Zhang, Y, Baumgartel, K, Mansuy, IM & Daw, NW (2005). Reversible blockade of experience-dependent plasticity by calcineurin in mouse visual cortex. *Nat Neurosci* 6, 791-796, DOI: 10.1038/nn1464.

Zhou, Q, Godwin, DW, O'Malley, DM & Adams, PR (1997). Visualization of calcium influx through channels that shape the burst and tonic firing modes of thalamic relay cells. *J Neurophysiol* 5, 2816-2825.

Zhou, Q, Homma, KJ & Poo, MM (2004). Shrinkage of dendritic spines associated with long-term depression of hippocampal synapses. *Neuron* 5, 749-757, DOI: 10.1016/j.neuron.2004.11.011.

Ziburkus, J, Dilger, EK, Lo, FS & Guido, W (2009). LTD and LTP at the developing retinogeniculate synapse. *J Neurophysiol* 6, 3082-3090, DOI: 10.1152/jn.90618.2008.

Ziburkus, J & Guido, W (2006). Loss of binocular responses and reduced retinal convergence during the period of retinogeniculate axon segregation. *J Neurophysiol*, DOI: 10.1152/jn.01321.2004.

Ziburkus, J, Lo, FS & Guido, W (2003). Nature of inhibitory postsynaptic activity in developing relay cells of the lateral geniculate nucleus. *J Neurophysiol* 2, 1063-1070, DOI: 10.1152/jn.00178.2003.

Vita

Emily Kathleen Dilger was born on May 12, 1982, in Cambridge, England, and is an American citizen. She graduated from Ward Melville High School, Setauket, New York in 2000. She received her Bachelor of Science in Biology from Mary Washington College, Fredericksburg, Virginia in 2004 and subsequently worked as a Research Assistant to Dr. Laurent Lecanu in the Department of Biochemistry at Georgetown University, Washington, D.C. for two years.

Publications

1. Song Y, **Dilger EK**, Chen H, Bell J, Barton W, Fang X (2010). Large scale purification and characterization of recombinant human autotaxin/lysophospholipase D from mammalian cells. *BMB Reports* 43, 541-46.

2. Bickford ME, Slusarczyk A, **Dilger EK**, Krahe TE, Kucuk C, Guido W (2010). Synaptic development of the mouse dorsal lateral geniculate nucleus. *The Journal of Comparative Neurology* 5, 622-635.

3. Ziburkus J, **Dilger EK**, Lo FS, Guido W (2009). LTD and LTP at the developing retinogeniculate synapse. *Journal of Neurophysiology* 102, 3082-90.

4. Dolby A, Temple J, Williams L, **Dilger EK**, Stechler K, Davis V (2004). Facultative rest-phase hypothermia in free-ranging white-throated sparrows. *The Condor* 2, 386-390.

Publications in Preparation

1. **Dilger EK**, Shin HS, Guido W. Requirements for synaptically evoked plateau potentials in relay cells of the dorsal lateral geniculate nucleus of the mouse. Submitted to Journal of Physiology.

2. **Dilger EK**, Morhardt DR, Shin HS, Guido W. The absence of synaptically evoked plateau potentials in dorsal lateral geniculate nucleus relay cells leads to a breakdown in retinogeniculate refinement.

3. Krahe TE, El-Danaf RN, **Dilger EK**, Henderson SC, Guido W. Morphologically distinct classes of relay cells exhibit regional preferences in the dorsal lateral geniculate nucleus of the mouse. Submitted to Journal of Neuroscience.

Awards

Osterud Award, Virginia Commonwealth University, 2010

Graduate Student Chapters Travel Award, Society for Neuroscience Annual Meeting: Chicago, IL, 2009

Phi Kappa Phi Scholarship, 2009

Spencer Neuroscience Award, Virginia Commonwealth University, 2009

Clayton Award, Virginia Commonwealth University, 2008